CHALMERS
UNIVERSITY OF TECHNOLOGY

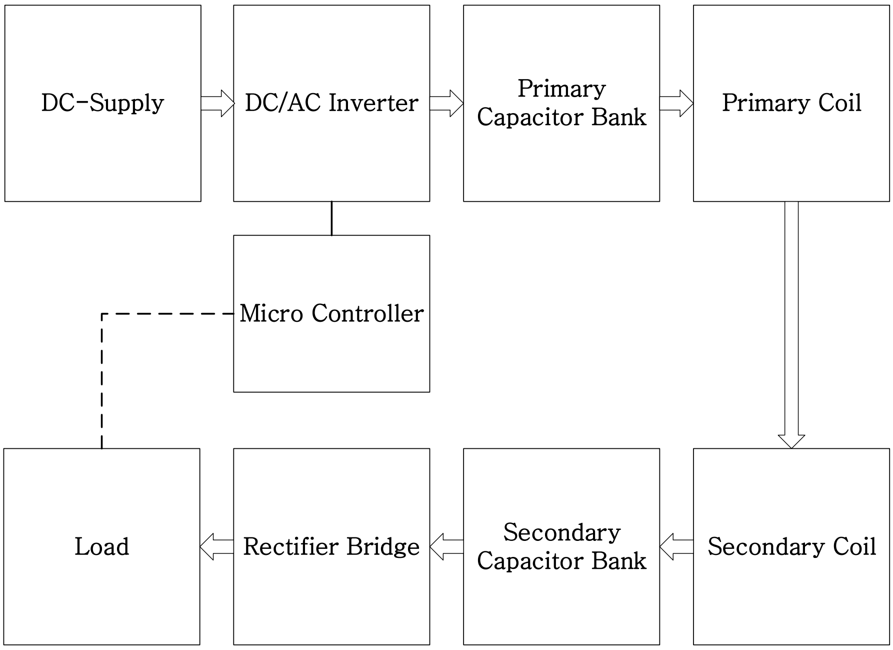

High efficiency inductive charging for electric mini-cars

System design and prototype development of a charging system

Master's thesis in Electric Power Engineering

PETTER MATTSSON
KIM OLSSON

Department of Energy and Environment
CHALMERS UNIVERSITY OF TECHNOLOGY
Gothenburg, Sweden 2015

Master's thesis 2015:06

High efficiency inductive charging for electric mini-cars

System design and prototype development of a charging system

PETTER MATTSSON
KIM OLSSON

Department of Energy and Environment
Division of Electric Power Engineering
Chalmers University of Technology
Gothenburg, Sweden 2015

High efficiency inductive charging for electric mini-cars
System design and prototype development of a charging system
PETTER MATTSSON
KIM OLSSON

Supervisor: Yujing Liu, Department of Energy and Environment
Examiner: Yujing Liu, Department of Energy and Environment

Master's Thesis 2015:06
Department of Energy and Environment
Division of Electric Power Engineering
Chalmers University of Technology
SE-412 96 Gothenburg
Telephone +46 31 772 1000

Cover: An overview of the parts in the charging system.
Typeset in LaTeX
Printed by Chalmers Reproservice
Gothenburg, Sweden 2015

High efficiency inductive charging for electric mini-cars
System design and prototype development of a charging system
PETTER MATTSSON
KIM OLSSON
Department of Energy and Environment
Chalmers University of Technology

Abstract

One way to reduce pollution from the vehicle fleet is to electrify it. Electric vehicles needs to be charged quite often and a conductive charger with a plug has several disadvantages compared to wireless charging. This thesis describes the simulation and development of an inductive charger to a small electric vehicle. The charger can transfer 700-950 W at an efficiency of 87 %, and 1100-1200 W at an efficiency of 84 %. Measurements shows that the most significant contribution to losses occur in the secondary coil. An efficiency of 90 % is possible if the design of the secondary coil is improved. To deal with the high leakage inductance of the coils, resonant capacitor banks are placed in series with each coil. The load current is regulated by changing the duty cycle of the inverter. Further work is however needed for implementation of automatic control. Tests has been performed where the two coils are misaligned and when the gap has been increased. Results shows that a misalignment of 100 mm will give a total efficiency of 80 % which is still good. As the system has shown good performance the technology should be viable for charging vehicles but could also be applied in other areas.

Keywords: Inductive power transfer (IPT), Wireless charging, Resonance, Electric vehicle, Inductive charging.

Acknowledgements

We would like to thank our examiner Yujing Liu for the guidance and help in the project. Without his ideas and mind we would never have gotten this far. A thank you goes out to Odysseas Lykartsis for providing hardware and support throughout the project with both simulations and testing of the system. We also thank Daniel Pehrman for sharing his knowledge and giving us input to the project which has led us forward. Lastly we would also want to thank William Collings and Jesper Maertang for their expertise regarding the vehicle system and battery as well as their questions and input.

Petter Mattsson and Kim Olsson, Gothenburg, June 2015

Contents

List of Figures

List of Tables

1

Introduction

1.1 Background

Since the harnessing of electricity was discovered, the use of electric power has been increasing steadily. This growth stimulate development of technology. In the 19th century the discovery that electric current induces a magnetic field was made, and theories around this was developed (Maxwell's equations) [1]. One pioneer in the field was Nikola Tesla who experimented with spark-excited radio frequency resonant transformers, with which he was able to transmit power over small air gaps. By these experiments he managed to transfer enough power through air to light a incandescent light bulb [2].

Inductive power transfer (IPT) has been used over the years in applications like charging of electric toothbrushes and induction ovens. Advancements of IPT includes charging mobile phones and cameras inductively, inductive heating and propulsion of trains by an electromagnetic circuit. As more portable electrical devices are developed the demand on charging increases. A lot of companies have developed their own charging solutions but the trend is leaning towards standardization of charging across all markets. Using electric vehicles is a way to reduce the world's consumption of non-renewable sources which today is around 80 % [3]. Electric vehicles often have an on-board charger with a plug that connects to the electrical grid. There are several disadvantages with this solution such as risk for sabotage, exposure to weather, stationary charging and the slight discomfort of plugging in to charge every time it is needed [4].

Inductive charging has many promising properties such as ease of use, cable-free charging of electric vehicles and charging on road during stops or during movement. This is a promising solution for charging and power transfer in many applications since it can easily be automated and standardized. The use of inductive power transfer in this project will include development and prototyping of an inductive charger for a small and light electric vehicle. The vehicle has a small battery which needs to be charged more frequently than for a full-sized electric car. IPT is tested on a smaller vehicle to get a basic understanding of the technology since a smaller vehicle will use a smaller design.

The small electric vehicle has three wheels and is registered as an EU-moped in Sweden. Data for the existing vehicle system is presented in Table 1.1.

Table 1.1: Data of the studied vehicle studied for the inductive charging.

Property	Value
Weight of vehicle	270 kg
Maximum charging current	90 A
Battery voltage	48 V
Power of drive train	2 kW
Battery capacity	2 kWh
Power of on-board charger	800 W
Available space for onboard receiver	300x300 mm

1.2 State of art technologies and market expectations

During the last decades a lot of research and development has been made in the field and IPT systems are used in the industry for example in vehicle assembly and clean rooms. IPT systems have benefits compared to traditional conductive charging since the systems are less affected by the weather, no moving parts or cables that are protruding for example. These benefits are especially suitable for electric vehicles. Electric vehicles can be charged when they are stationary or even while driving on a road with built in charging units. There has been several projects aiming towards electric vehicles and IPT and Table 1.2 summarizes a few.

Table 1.2: Summary of IPT projects toward the electric vehicle area. Power level, efficiency, vehicle type and air gap are presented for the projects. Efficiency numbers for ORNL is defined as Coil-to-coil, all others are for the entire system.

Institute/Corporation	Year	Vehicle type	Power level	Air gap	Efficiency
The University of Auckland	1997	5 Golf buses	20kW	50mm	90-91%
	2003	8-23 mini buses	60kW	30mm	-
	2010	Private vehicles	3kW	180mm	85%
Oak Ridge National Laboratory (ORNL)	2010	-	4.2kW	254mm	92%
	2012	-	7.7kW	200mm	93%
	2012	GEM EV	2kW	75mm	91%
Korea Advanced Institute of Science and Technology (KAIST)	2009	Golf bus	3kW	10mm	80%
	2009	Bus	6kW	170mm	72%
	2009	SUV	17kW	170mm	71%
	2010	Tram	62kW	130mm	74%
	2012	Bus	100kW	200mm	75%
MIT WiTricity	2010	Private vehicles	3.3kW	180mm	90%

It can be seen in Table 1.2 that the power range is around 3 kW and upwards to 100 kW. There is a lack of research in the range between electric toothbrushes and to a few kW for medium power applications. The projects have all been performed with different vehicle types, air gaps and power levels. It can also be seen that very high power (100 kW) has been transferred over a air gap as large as 200 mm which shows the viability of IPT as a charging solution.

As the technology has advanced, focus has been improving the design of power supplies to achieve high efficiency at high switching frequencies and power levels. Improvements of the magnetic circuits has also been made to achieve a higher efficiency and wider range of operation with higher tolerance to misalignment. The pads have evolved from conventional circular pads to more complex pads with two or three windings which gives a larger operating area and higher power delivery for roughly the same size of the power pads.

The total market for inductive charging for electric vehicles is anticipated to grow with a CAGR (Compound Annual Growth Rate) of 126.6 % from 2012 to 2020 according to the market analysis done by Frost & Sullivan in 2014 [5]. Europe will be the market leader in IPT solutions by 2020 followed by the United States mainly because of the adoption rate of electric vehicles but also since OEMs such as Volvo Car Corporation, BMW AG, Bombardier and Qualcomm are achieving technological advances in the field. There are a few aftermarket products available for purchase at the market today and Frost & Sullivan predicts that the first electric vehicle with built-in IPT should hit the market in 2015 and most OEMs should offer IPT on cars after 2016. They also predict that IPT solutions for stationary application will be popular and that dynamic charging will be popular for public transportation after 2020. The power level of IPT systems are for know set at 3.3 kW but the trend is inclined towards 6.6 kW with higher power levels mostly used for dynamic charging of larger vehicles. OEMs are also developing the standard SAE J2954 jointly to establish minimum performance for efficiency and develop safety criteria for wireless charging of electric vehicles. They develop the standard by evaluating technologies and compiles this to the standard.

1.3 Aim

A general purpose behind this project is to demonstrate the feasibility of IPT for a small electric vehicle (EV) by designing a prototype inductive charger which is low-cost and highly efficient. The charger will be tested on the battery used by the vehicle to verify the design and topology selected. The charger will be capable to control the battery charging based on the battery level. The power level of the charger should be at least 800 W. The system efficiency from grid to battery is aimed to be higher than 80 %. The size of the onboard receiver should be designed to fit inside the vehicle. The proposed system together with the already existing charger is visualized in Figure 1.1.

1.4 Scope

This project will be carried out in close relation with another Chalmers project regarding inductive rotor excitation. Due to the close nature of these two projects, similar hardware components will be used in both projects. The possible effects of this are a lower efficiency of the power electronic part of the charger. The choice of using the same hardware is however motivated due to the tight time schedule, there is simply not enough time to design new components. This means that the

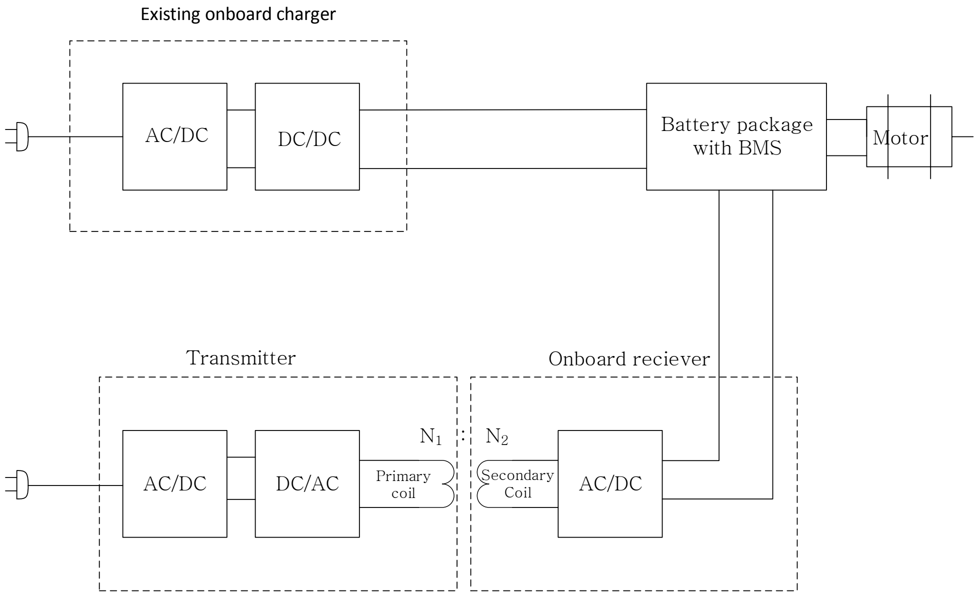

Figure 1.1: Overview of the charging and drive system of the intended vehicle. The transmitter and on board reciever is the parts that will be developed in this project.

design of the inverter will not be performed since this is made in the other project. Communication with the BMS for control will be done late in the project if there is enough time left. Radio link is one possible solution as a mean of communication. The structure and layout of the system will not have a high priority and the air-gap between the power pads will be lower than in full-sized vehicles. The dimensions of the power pad will be restricted by the free floor area in the vehicle. Thermal calculations during operation and a study of optimal power pad topology will also not be conducted although the temperature of components will be monitored.

2

Methods

A literature study will be conducted by using online resources as well as printed sources. The literature study will be the base knowledge to be able to perform design decisions. Calculations and simulations will be done to determine detailed dimensions and parameters for the design. The rectifier, inverter and resonant circuit designs will be evaluated in terms of efficiency, cost, complexity and ease of use. A optimal pad design will be chosen based on a study of different designs. The selected design will be simulated with COMSOL and LTSpice.

The power electronics will be assembled in the lab since they need to fit the application. The pad will be assembled in the lab by using ferrite materials in the chosen form and by already existing wire. The capacitors that are available in the lab will be evaluated if they suit the designed resonance circuit, otherwise suitable capacitors will be bought and assembled.

The system will be evaluated by measurements to find the efficiency and power transfer. An estimation of the produced magnetic field will be done to ensure that safety standards are met as well as a good distribution and utilization is achieved. Simulations and calculations will also be done after the system is assembled to see if better solutions might be found and parts of the system improved. Testing of the prototype charger will be conducted both on power resistors as load and on the real battery that is used by the electric car.

3

Introduction to inductive power transfer (IPT)

This chapter will introduce concepts needed to understand inductive power transfer and explain the theory behind it. How a battery should be charged is also mentioned as well as health and regulations regarding magnetic fields.

3.1 The concept of induction

Faradays law stated in (3.1) is the fundamental postulate for electromagnetic induction. It states that an electric field E in a region containing a time-varying magnetic flux density B is non-conservative.

$$\nabla \times E = -\frac{dB}{dt} \tag{3.1}$$

By taking the surface integral and applying Stokes theorem, (3.1) can be written as

$$\oint_C E \cdot d\ell = -\frac{d}{dt}\int_S B dA \tag{3.2}$$

which is valid for every geometrical body with a surface S and a contour C. The magnetic flux Φ can be written as

$$\Phi = \int_S B dA \tag{3.3}$$

and the electromotive force emf, which is a voltage that try to negate the electric field induced in a circuit, can be defined as

$$emf = \oint_C E \cdot d\ell. \tag{3.4}$$

Combining (3.3) and (3.4) gives

$$emf = -\frac{d\Phi}{dt} \tag{3.5}$$

which states that the time varying magnetic flux that links a circuit will induce an emf. The negative sign means that the induced emf will drive a current which will oppose the change in the magnetic flux.

In the same way that a time-varying magnetic field linking a looped circuit will give rise to an induced current, a time-varying current trough a looped circuit will give rise to a time-varying magnetic field. This relation is used in a transformer [6].

3.2 The concept of inductance

Two closed loops are shown in Figure 3.1. According to the Biot-Savart law

$$B_1 = \frac{i_1 \mu_0}{4\pi} \oint_{C1} \frac{d\ell \times \hat{\mathbf{r}}}{r^2} \tag{3.6}$$

the current i_1 that flows in the first loop will create a magnetic field density B_1. μ_0 is the permeability constant and r is the radius of the closed loop.

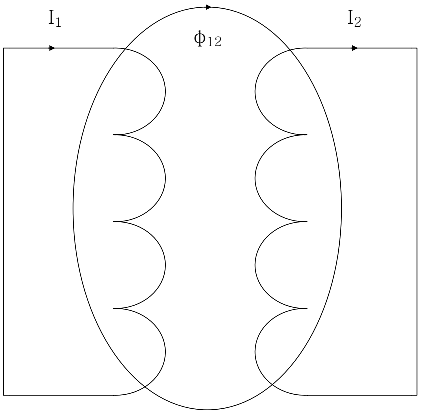

Figure 3.1: Two loops with a magnetic coupling and the currents flowing in each loop.

The part of the magnetic field density that passes through the surface S_2 of the second loop is denoted the mutual flux Φ_{12} and can be calculated as

$$\Phi_{12} = \int_{S2} B_1 \cdot \mathrm{d}s. \tag{3.7}$$

By looking at (3.6) and (3.7), it is clear that the mutual flux Φ_{12} is proportional to the current i_1. This relation can be written as

$$\Phi_{12} = M i_1 \tag{3.8}$$

where the constant M is called the mutual inductance between the loops and is measured in Henry [H]. If the second loop has multiple turns N_2, the flux linkage will be

$$\Lambda_{12} = N_2 \Phi_{12} \tag{3.9}$$

which when used in (3.8) gives

$$M = \frac{\Lambda_{12}}{i_1 N_2}. \tag{3.10}$$

The mutual inductance can also be written in terms of i_2 and Λ_{21},

$$M = \frac{\Lambda_{21}}{i_2 N_1}. \tag{3.11}$$

Similarly to mutual inductance, the self inductance L can be defined. The self inductance of the first loop in Figure 3.1 is defined as the flux linkage with the loop itself per unit current, i.e

$$L_1 = \frac{\Lambda_{11}}{i_1}. \tag{3.12}$$

The self inductance does not depend on the current for linear mediums, instead it is the geometrical shape of the loop that determines the inductance. By having the mutual inductance and the self inductance of the two coils it is possible to define the coupling factor k,

$$k = \frac{M}{\sqrt{L_1 L_2}}. \tag{3.13}$$

In an ideal transformer, all the flux that links with the primary loop will also link with the secondary loop. This means that the self inductance will be equal to the mutual inductance and $k = 1$. In a IPT system however, the coupling is poor and the leakage inductance is several times larger than the mutual inductance.

3.3 Transformer model

In an ideal transformer, all the flux created by the current in the primary winding are linking with the secondary winding. This is however not the case when dealing with a real transformer. The leakage inductance L_σ in a transformer is the magnetic flux created by one coil that doesn't link with the other coil. The relation between the self inductance, mutual inductance and leakage inductance are

$$L_1 = L_{\sigma 1} + M. \tag{3.14}$$

Figure 3.2 is showing the equivalent model of a transformer with winding losses. The voltage V_1 can be written as

$$V_1 = R_1 i_1 + (M + L_{\sigma 1})\frac{di_1}{dt} - M\frac{di_2}{dt} \tag{3.15}$$

and V_2 as

$$V_2 = -R_2 i_2 - (M + L_{\sigma 2})\frac{di_2}{dt} + M\frac{di_1}{dt}. \tag{3.16}$$

According to the ideal transformer model, the winding resistance and the leakage inductance can be transferred from the secondary side to the primary side as

$$Z_2' = (\frac{N_1}{N_2})^2 Z_2 \tag{3.17}$$

Further, the mutual inductance can be represented as a magnetizing inductance L_M which represent the nonlinear magnetization behavior

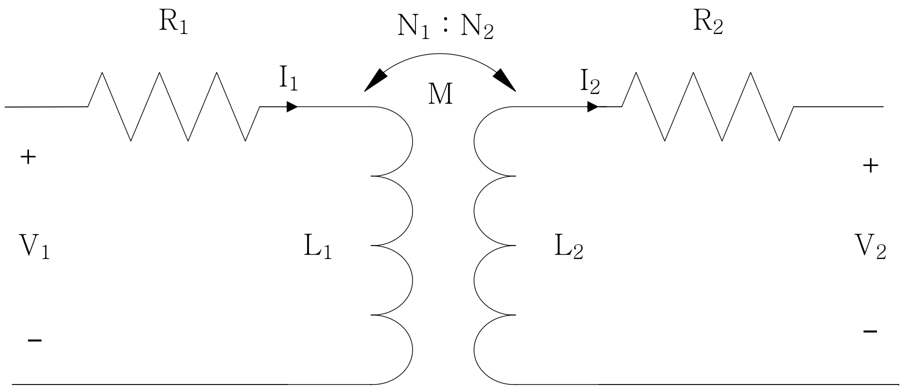

Figure 3.2: A simple transformer model which shows the coupling between the two coils. The input and output voltage and currents as well as the coil resistance and inductance are visible.

$$L_M = \frac{N_1}{N_2} M \tag{3.18}$$

Using these relations, the transformer model in Figure 3.2 can be represented by the circuit in Figure 3.3 where R_2 and $L_{\sigma 2}$ are transferred to the primary side of the transformer. The load current I_2 and the voltage V_2 over the load can then be transferred to the primary side using ideal transformation. This model can be properly used for analytical calculations and simulations [6].

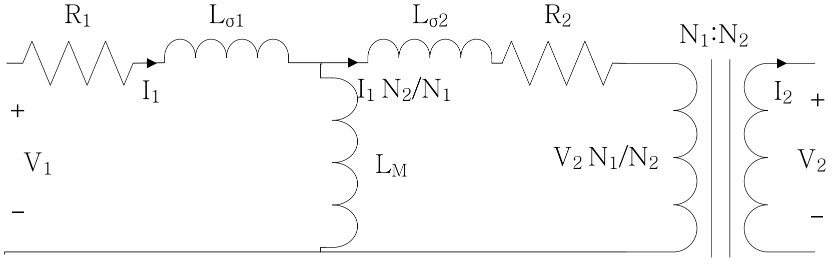

Figure 3.3: A circuit model of the transformer which is suitable for calculations and simulations. R_2 and $L_{\sigma 2}$ are transferred to the primary side.

3.4 Resonant circuit

Figure 3.4 shows a simple circuit containing a resistor and two energy storage elements in series, one inductor and one capacitor. The total impedance of the circuit is

$$Z = j\omega L + \frac{1}{j\omega C} + R \tag{3.19}$$

which can be arranged in to a reactive part and a resistive part

$$Z = R + j\frac{\omega^2 LC - 1}{\omega C}. \tag{3.20}$$

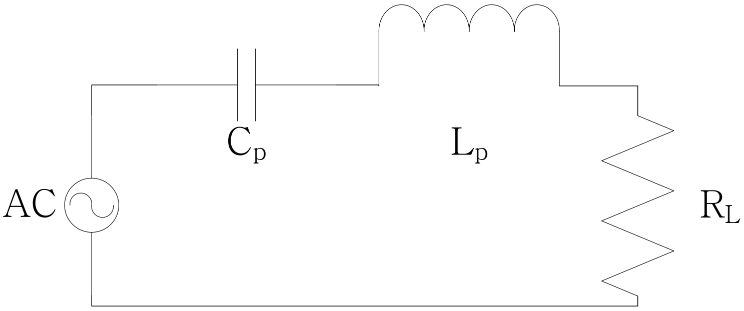

Figure 3.4: Resonant circuit with the energy storage elements in series.

At a certain frequency ω_0, the numerator in (3.20) will be equal to zero and hence, the total impedance will be fully resistive. This frequency is called the resonance frequency and is written as

$$\omega_0 = \frac{1}{\sqrt{LC}} \tag{3.21}$$

Figure 3.5 shows a resistor together with a capacitor and an inductor connected in parallel. The total impedance is

$$Z = \frac{\omega^2 C^2 R}{1 - 2\omega^2 CL + \omega^4 C^2 L^2 + \omega^2 C^2} + j\frac{\omega CR - \omega^3 C^2 LR}{1 - 2\omega^2 CL + \omega^4 C^2 L^2 + \omega^2 C^2} \tag{3.22}$$

The impedance will be entirely resistive, i.e $Z = R$, when the numerator of the reactance is zero,

$$\omega CR - \omega^3 C^2 LR = 0 \tag{3.23}$$

This gives the resonance frequency

$$\omega_0 = \frac{1}{\sqrt{LC}} \tag{3.24}$$

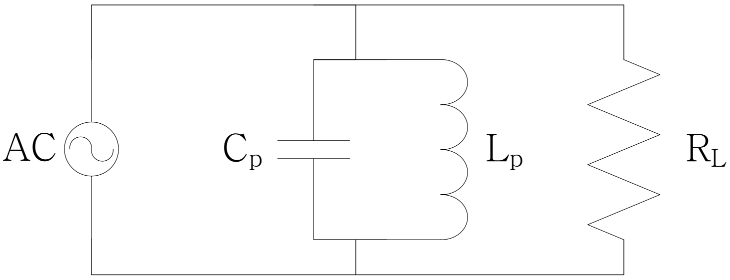

Figure 3.5: Resonant circuit with the energy storage elements in parallel.

3.4.1 Quality factor of resonant circuit

The quality factor in a system is a measure on how fast oscillations will damp out. A system with a high quality factor will have less damping but will resonate with a higher amplitude compared to a system with a lower quality factor. The bandwidth will be smaller with increasing Q-factor. The quality factor for a series resonant circuit is defined as

$$Q_s = \frac{1}{R}\sqrt{\frac{L}{C}} \tag{3.25}$$

and for a parallel resonant circuit as

$$Q_p = R\sqrt{\frac{C}{L}} \tag{3.26}$$

3.5 Resonant compensation topologies

As mentioned in Section 3.4, the resonant circuit can be arranged in primarily parallel or series. In IPT there is poor coupling between the primary and secondary side in the transformer. The poor coupling will lead to a high impedance when the frequency is high. A high frequency is essential in IPT to achieve an efficient power transfer. This will lead to a poor power factor which will stress the source inverter and force it to be rated for high apparent power which is unnecessary. To increase the power factor and thus the power transfer capability of the IPT capacitive compensations is added to both sides of the transformer. The purpose of compensation on the secondary side is to increase the power transfer capability and the primary side compensation to decrease the VA rating of the inverter by achieving a high power factor.

The compensation can be arranged in four basic topologies, Parallel-Parallel (PP), Series-Series (SS), Parallel-Series (PS) and Series-Parallel (SP). All of which have different characteristics and effects on the circuit. To achieve high power transfer the operational frequency should be the secondary side resonance frequency ω_0. If the circuit is operating at that frequency the inductance of the secondary side is fully compensated by the secondary side capacitor C_2 and the impedance of the secondary side will be seen as resistive from the primary. This means that the secondary side capacitance C_2 is defined as

$$C_2 = \frac{1}{\omega_0^2(L_{\sigma 2} + L_M)} \tag{3.27}$$

for all topologies above. The compensation on the primary side is chosen so the inverter operates at unity power factor i.e the input voltage and current are in phase. The primary side capacitor will therefore be chosen differently depending on the topology.

3.5.1 Parallel-Parallel topology

Parallel-Parallel is often mentioned as a good choice for charging of batteries since it will act as a voltage source. The primary side capacitance C_1 is defined as

$$C_1 = \frac{(L_{\sigma 2} + L_M)^2((L_{\sigma 1} + L_M)(L_{\sigma 2} + L_M) - L_M^2)C_2}{((L_{\sigma 1} + L_M)(L_{\sigma 2} + L_M) - L_M^2)^2 + L_M^4 R_L^2 (L_{\sigma 2} + L_M) C_2} \tag{3.28}$$

where $L_{\sigma 1}$ and $L_{\sigma 2}$ is the leakage inductance on primary and secondary side, L_M the magnetizing inductance and R_L the load resistance [7].

3.5.2 Series-Series topology

This compensation topology will act as a current source which is suitable for battery charging since the current supplied will not change as the load changes. One advantage of the SS topology is that when operating at the secondary resonance frequency ω_0 the reflected impedance of the secondary winding will be resistive but also that the primary compensation is independent of the load [7]. For this compensation the primary capacitor is defined as

$$C_1 = \frac{(L_{\sigma 2} + L_M)C_2}{(L_{\sigma 1} + L_M)} \tag{3.29}$$

where $L_{\sigma 1}$ and $L_{\sigma 2}$ is the leakage inductance on primary and secondary side, L_M the magnetizing inductance and C_2 is the secondary compensation capacitor as calculated in (3.27) [7].

3.6 Charging characteristics of Li-ion battery

There exist several methods of battery charging, and the method of charging often depends on the specific type of battery that is to be charged. In this application the battery that will be charged is a Lithium-Ion (Li-Ion) battery. The charging of a Li-Ion cell can be divided in two stages; Constant current (CC) and Constant voltage (CV). During the CC stage a constant current is delivered to the battery and during this stage the voltage of the battery will increase. When the battery has reached its maximum cell voltage (normally 4.2 $V/cell$ for Li-Ion) the charging should change to the CV stage where a constant voltage equal to the maximum cell voltage is applied and the charging current will decrease. When the charging current has reached 3 % of the rated current the battery is considered fully charged.

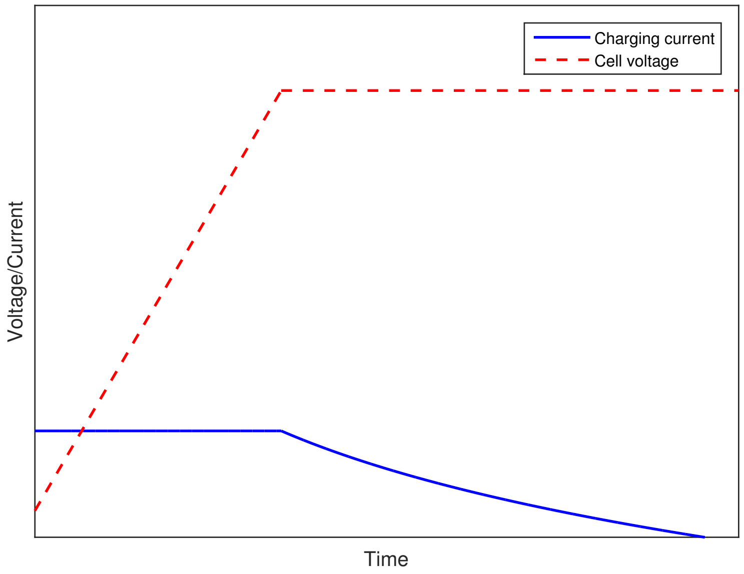

Figure 3.6: Charging characteristic for Li-Ion battery. The battery is charged with a constant current until it reaches its maximum cell voltage. At the maximum voltage point the current is decreased and the applied voltage is constant.

3.7 Health aspects and regulations of magnetic fields

As the system consist of a loosely coupled transformer not all magnetic flux will be coupled which leads to leakage flux. The leakage flux will not only cause losses in the system but can also be an issue to health. There are guide lines summarized by Strålskyddsmyndigheten (Swedish Radiation Safety Authority) which set reference values for maximum field strength and flux densities in public space. The maximum values of these quantities at 100 kHz are 5 A/m and 6.25 μT for the field strength and flux density respectively [8].

The magnetic fields can induce circulating currents to a body that is exposed. The magnitude of the induced currents depend on the magnetic field strength and for high magnitudes nerves or other biological tissue might be affected. Heating of tissue may also occur at high frequencies and this is the basis for the regulations that exist for magnetic fields. There is debate in the area but no negative health effects caused by low level exposure have yet been found, however there is still active research in the area.

4

Power Electronics

This chapter presents the power electronics used in the system. The inverter section contains information about the MOSFETs and gate drivers that were used. The model of the inverter that was implemented in LTSpice is also presented.

4.1 DC/AC inverter

A full bridge inverter is used to supply the transformer circuit with a high frequency voltage. The inverter is primarily designed for another project regarding wireless excitation of an electric motor, but since both projects have similar power and frequency levels, it possible to use the inverter for this project as well. Figure 4.1 shows a simple circuit model of a full bridge inverter.

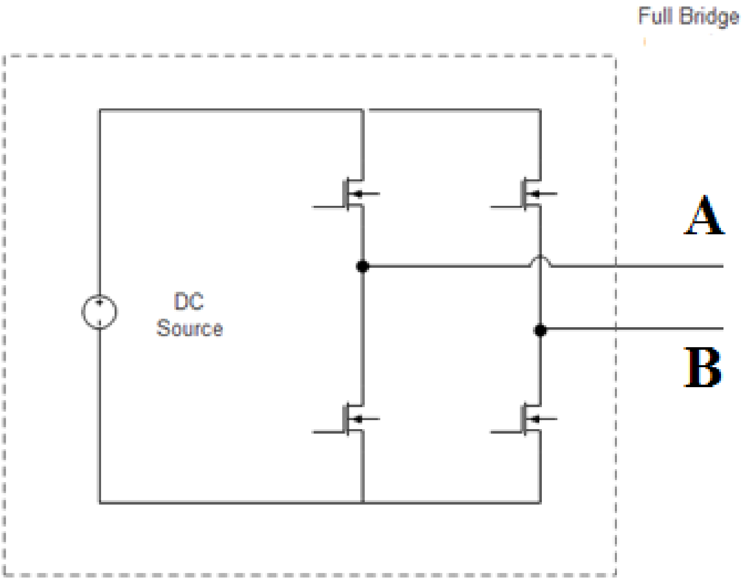

Figure 4.1: A simple illustration of an full-bridge inverter. It consist of four switches, two for each leg.

The models of the MOSFETs that are used in simulations are downloaded from the manufactures website, and these are described later in this section. The inverter uses square wave operation with the output voltage controlled by voltage cancellation. Square wave operation is a more simple solution than pulse-width modulation, but a drawback is the higher harmonic content in the output. Figure 4.2 shows the voltage potential between point A and ground and point B and ground. Both square waves has a duty ration of 0.5 and the amplitude of the square waves are equal to the DC link voltage. This corresponds to an angle of 180 degrees for both V_A and V_B, with a full period corresponding to 360 degrees. The resulting output voltage from the inverter is the difference $V_A - V_B$ and is shown in Figure 4.3.

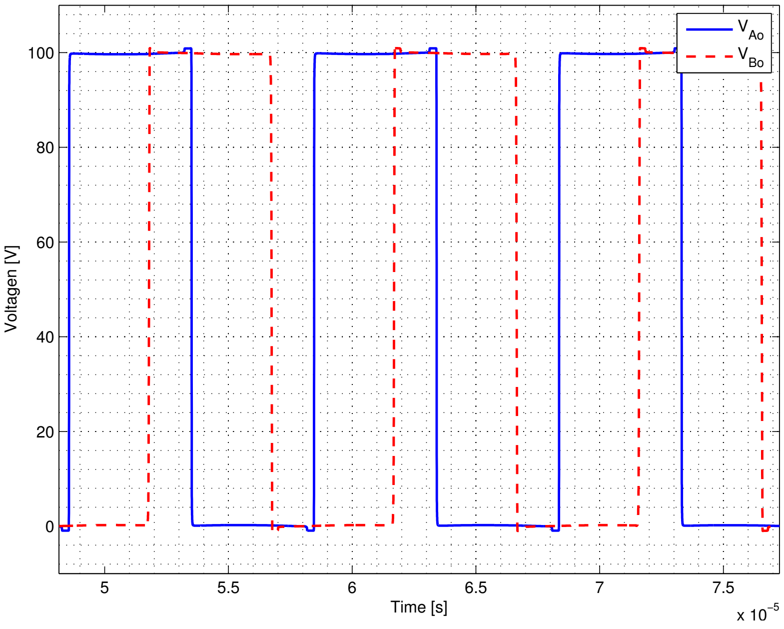

Figure 4.2: The voltage at point A and B to ground.

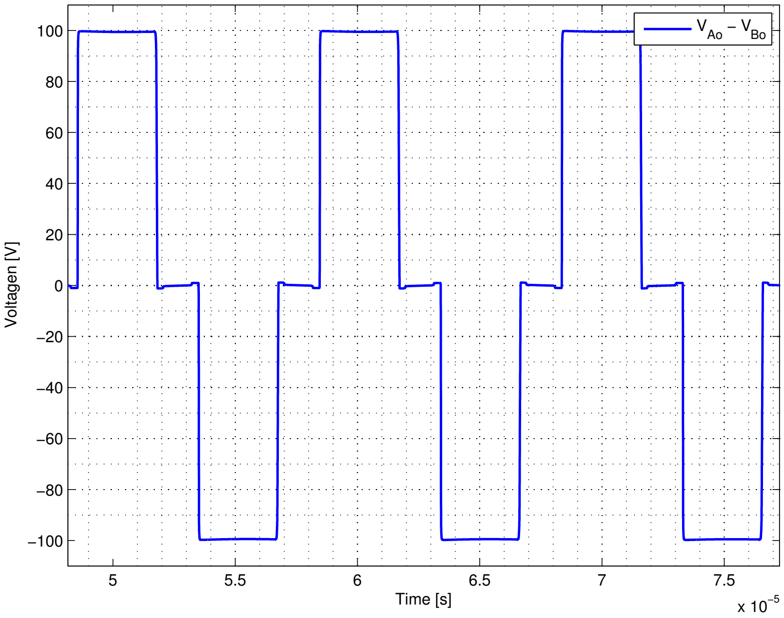

Figure 4.3: The resulting output voltage from the inverter is the difference $V_A - V_B$.

The RMS value of the output voltage is regulated by controlling the angle that the two pulses overlap each other with. This overlap is achieved by having either both top switches on or both bottom switches on simultaneously which gives a zero output voltage. In Figure 4.2, the overlapping angle corresponds to 54 degrees phase shift between the two voltages. With no overlap, the RMS value of the output voltage is equal to the DC link voltage. When having an overlap angle α, the RMS value of the output voltage is given by

$$V_{RMS} = V_{DC}\frac{180 - \alpha}{180} \tag{4.1}$$

The factor $\frac{180-\alpha}{180}$ corresponds to the duty ratio of the output voltage $V_A - V_B$ [9].

4.1.1 Switches used in the inverter

The switches used in the inverter are SCH2080KE SiC n-channel MOSFETs. SiC stands for silicon carbide and is quite new to the market. The benefits with silicon carbide MOSFETs is its higher temperature ratings compared to old silicon MOSFETs. Table 4.1 summarizes the most important ratings of SCH2080KE at $T = 25\ °C$.The current and voltage ratings are higher than the intended operation point and will thus give a safety margin. A smaller R_{DSon} would decrease the conduction losses, but this would also give a larger output capacitor. The importance of a small output capacitor is described in Section 4.5.

Table 4.1: Summary of SCH2080KE ratings.

Parameter	Value
V_{DSS} [V]	1200
R_{DSon} [$m\Omega$]	80
I_D [A]	40
C_{OSS} [pF]	175

4.1.2 Gate Driver topology

The inverter uses totem pole gate drivers which are cable to provide a bipolar output. Bipolar gate drivers can provide both positive and negative outputs and will give a shorter turn-off time compared unipolar gate drivers [9].

4.1.3 Losses in inverter

The inverter will contribute with losses to the system when it is conducting as well as when the switches are operating. These losses can be hard to evaluate correctly but it is good to at least find a close approximation of them. The total losses in the inverter can be expressed by

$$P_{Inverter} = P_{COND} + P_{SW} \tag{4.2}$$

where P_{COND} is the total conduction losses for the switches and P_{SW} is the sum of the on- and off-switching losses for the switches. The conduction losses for one switch can be calculated by

$$P_{COND} = \frac{1}{T}\int_{t_{on}}^{t_{off}} V_{DS}(t)I_D(t)dt \approx I_D^2 R_{DS,ON} D \tag{4.3}$$

where t_{on} is the time when $V_{DS}(t)$ has decreased to zero and t_{off} is the time when that voltage starts to increase again. $R_{DS,ON}$ is the on-state resistance in the switch and D is the duty cycle for the switch. The time interval t_{off} - t_{on} is when the switch is closed and conducts a current. For a full bridge layout there is four switches and two will always conduct at the same time. The total conduction losses will therefore be four times the conduction losses that one switch is contributing to. When the switches are transitioning between on- and off-state losses will also occur since the voltage and current through the switch often change simultaneously. The switching losses for either the on- or off-switching can be evaluated as

$$P_{SW} = \frac{1}{T}\int_{t_1}^{t_2} V_{DS}(t)I_D(t)dt \tag{4.4}$$

where t_1 is the time where the current starts to rise and t_2 is the time when the voltage V_{DS} reach zero for the on-switching and the reverse for the off-switching state. The switching losses for one switch will therefore be the sum of the on-switching losses and the off-switching losses. The total switching losses will be the sum of on- and off-switching losses for four switches in a full bridge layout.

4.2 Micro controller

To control the switching of the inverter a signal must be sent to the gate drive circuit. The signal to the gate drive circuit is created in a micro controller and is a digital signal which describes the switching timings and frequency the inverter should use. The micro controller used in this project is a evaluation board from Texas Instruments called C2000 Piccolo LaunchPad which is based around C2000 Piccolo TMS320F28027 MCU. This microcontroller was chosen since it is pre-programmed with a lot of functions and it is easy to access the MCU through pins. The board has a USB interface which makes reprogramming and real time control easy when using a computer. If the micro controller is connected to a computer real time control can be performed by changing variables such as the duty cycle of the switching.

4.3 AC/DC Rectifier

To convert a AC to DC a rectifier is needed. The idea of rectification is to take an alternating voltage and convert it to a constant polarity. A rectifier basically consist of one or four diodes depending on if half wave or full wave rectification is wanted. Since a diode can only conduct positive currents, at the output of the diodes only the positive part of the alternating voltage will be seen. When four diodes are used the circuit is built in a way as can be seen in Figure 4.4 that enables the full wave to be seen at the output of the diodes as a positive voltage.

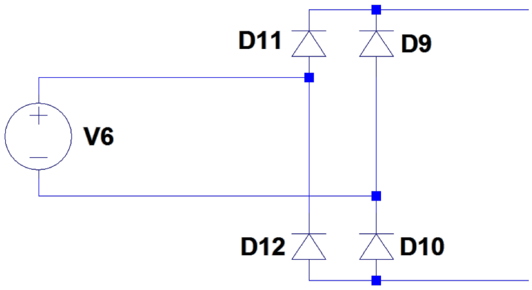

Figure 4.4: A rectifier circuit with a four diode bridge layout. This is a full wave rectifier with ideal diodes.

Figure 4.5 illustrates an alternating sine wave voltage and Figure 4.6 is showing the output voltage from a full wave rectifier. The DC voltage output from the rectifier can be calculated by

$$V_{dc} = \frac{2\sqrt{2}V_{ac,rms}}{\pi} \approx 0.9V_{ac,rms} \tag{4.5}$$

where $V_{ac,rms}$ is the input alternating voltage to the rectifier. If a capacitor is added this will be charged when the AC voltage is increasing and discharged after it reaches its peak until the AC voltage is the same value as the DC voltage, then the cycle repeats. V_{dc} can in this case become higher than its theoretical value from (4.5). Rectification can also be performed actively by using switches such as MOSFETs, this will often reduce losses in the rectification stage over diodes but the circuitry becomes more complicated.

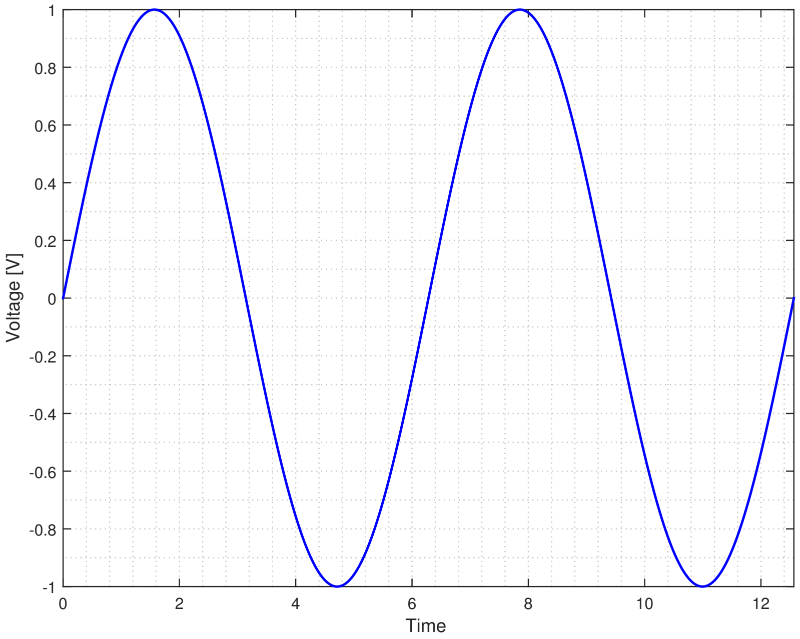

Figure 4.5: An alternating sine wave voltage.

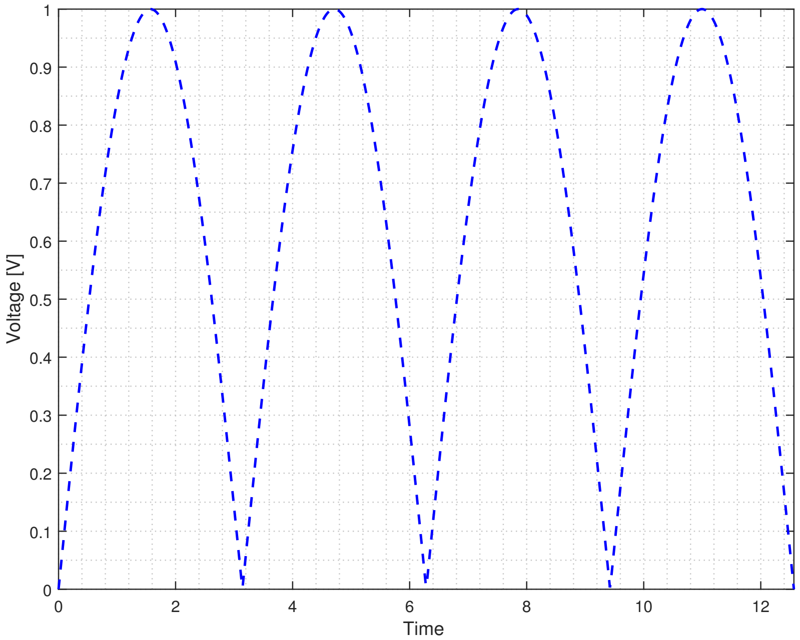

Figure 4.6: The sine wave after rectification.

4.3.1 Loss calculations of the rectification stage

To minimize the losses in the system the diodes in the rectifier should have a low forward voltage drop as well as a short reverse recovery time. The losses that occur in the rectifier will be conduction losses and reverse recovery losses as the diode stops conducting when the voltage over it changes polarity. The conduction losses is mainly dependent on the threshold voltage together with the average current that the diodes conducts. The slope of the diode characteristic and the RMS of the current will also contribute to the conduction losses. These losses can be calculated by

$$P_{conduction} = V_{T0} I_{F,AVG} + R_D I_{F,RMS}^2 \tag{4.6}$$

where V_{T0} is the threshold voltage, R_D is the slope resistance and $I_{F,AVG}$ as well as $I_{F,RMS}$ is the average and RMS value of the conducted current. The conduction losses depend on the temperature of the diode since the threshold voltage and slope resistance will decrease as the temperature increase. This is however often disregarded since it is hard to determine the exact values of the parameters for a specific operation. The manufacturer has specified which parameter values to use for loss calculation in the data sheet.

4.3.2 Load side rectification

As the intended use for the system is to charge a battery in a electric vehicle the supply voltage and current to this must be DC. Since the inverter generates a high frequency AC this must be rectified to supply the load. The rectification on the secondary side must handle the average of the charging current to the battery and also the maximum voltage that is induced in the secondary side of the transformer. The average charging current will be in the range of $20 - 30$ A, and the maximum voltage supplied has been measured to approximately 200 V. The diode package used for rectification on the secondary side in the system is named IXYS DSEI2x101-06A and is packaged with two diodes in a package that can handle quite high power. The most important ratings of the diode package are the maximum repetitive reverse voltage which is 600 V, and the average forward current rating which is 96 A per diode with a reverse recovery time of 35 ns.

4.4 Electromagnetic interference (EMI)

Electromagnetic interference are often generated in integrated circuits which is then coupled to conduction planes of the circuit board, cables or heatsinks [10]. It can be a complicated matter to reduce EMI but some examples are: decoupling capacitors or shielding. An IPT system includes switching devices that operate at a high frequency which creates noise that makes its way to measured signals as the measuring probes/cables will act as small antennas. In measurements the noise can be detected by identifying its frequency and can then be either filtered or just ignored. When using measurements to calculate other quantities the noise will not affect significantly since the energy content of it is low compared to the energy in the fundamental frequency of the signal.

4.5 Zero-Voltage switching

High switching losses is a downside when operating at high frequencies, which is the case for inductive charging. ZVS is achived by having the output capacitor of the switches resonate with some leakage or added inductance in the output circuit of the inverter during the switches off-time. It is preferable that the switches has a small output capacitor since this will lower the needed inductance of the output circuit that it will resonate with. The following relation must be fulfilled if ZVS is to be achieved

$$\frac{1}{2}C_{oss}V_{DC}^2 < \frac{1}{2}LI^2 \tag{4.7}$$

The voltage V_{DC} is the voltage at the DC link and the current I is the output current of the inverter. The meaning of (4.7) is that the magnetic energy in the inductor must be higher than the electric energy in the capacitor, and if it is fulfilled, the capacitor will be fully discharged during the off-time of the switches. The duty cycle plays an important role in ZVS since I but not V_{DC} in (4.7) is dependent on the duty cycle. If the duty cycle is increased, then I is increased but V will remain constant and hence, the right hand side of (4.7) will be increased and the left hand side will remain constant. Figure 4.7 illustrates the transition between off and on for one switch when having ZVS at a duty cycle of 0.9. Figure 4.7 can be compared to Figure 4.8 where the duty cycle is 0.4, which is not enough to achieve ZVS. The current in Figure 4.7 reaches negative values when it goes through the body diode. When the switch starts to conduct, the voltage V_{DS} has gone to zero which will give no switching losses [11].

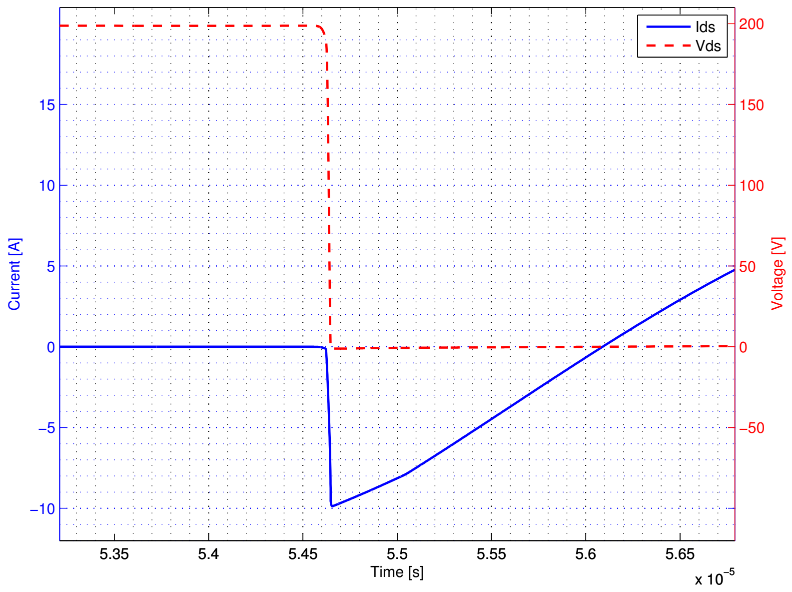

Figure 4.7: The figure shows the transition between off-state and on-state of one switch when having ZVS. The voltage has gone to zero befor the current starts to rise. The duty cycle is 0.9.

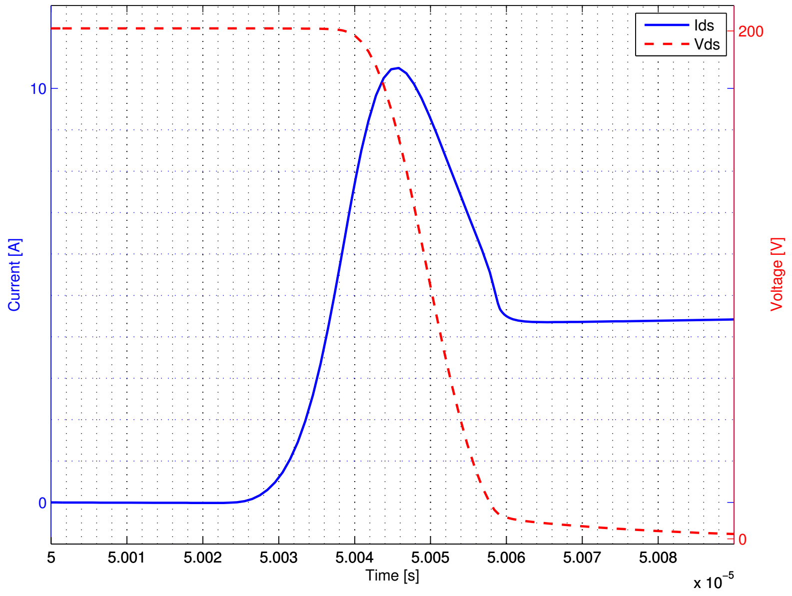

Figure 4.8: The figure shows the transition between off-state and on-state when having switching losses. The voltage is decreasing at the same time as the current is increasing. The duty cycle is 0.4.

5

Transformer design

To design the transformer there is many things to consider. The main limitation of the design is the available space on the vehicle and thus the size of the coils must be smaller than the given space. The design process is iterative in the way that when a possible design has been found it has been tested through circuit simulations to find if it fulfills the power level wanted for the transformer. The main part of the design has been made through FEM (Finite Element Method) simulations where the coils has been drawn and inductance of the coils has been calculated. The accuracy of the simulations was a concern and therefore comparison between two software's and analytical expressions was made.

The losses that occur in the transformer is mainly due to the resistance of the coils and the stray magnetic field. The coil resistance depends on several factors and will increase when the current through the coils have a high frequency. The resistance can be reduced by using a special type of wire, Litz wire, to wind the coils. The stray field in the transformer will induce currents in nearby metallic objects which will heat them up and cause losses. The field can to some degree be controlled by the design, mainly by adding ferrite to the coils which has a high permeability and can conduct the magnetic field well. There are also health effects caused by the magnetic field so the stray field must be minimized around the transformer to fulfill regulations.

5.1 FEM simulations

To have full understanding and control of the system the magnetic fields must be known. When designing the power transfer pads the geometry is an important design parameter since this will influence the inductance and resistance of the coils. When using ferrite in the design the magnetic flux inside the ferrite is important to minimize losses and improve performance. The circuit can be simulated in the same way as in a circuit simulation program but with focus on how the magnetic coupling behaves, thus the results from FEM and circuit simulations can be compared. The main goal of the FEM simulations are to find the coil inductance and also analyse the magnetic fields created. The magnetic fields must be monitored since there are safety regulations of stray fields and also to utilize the ferrite effectively without saturation.

5.1.1 Geometry of the transformer coils

The geometry of the coils are drawn in 2D space since it is fast to design and simulations can be conducted rapidly. The main limiting parameter is the outer radius of the power pad since the prototype should be fitted to the vehicle. The design was iterated several times while the calculated values was simulated in a circuit to find a suitable design that delivers the power wanted. In Figure 5.1 the two coils (orange fields) is visible as well as a layer of ferrite (black fields) and also a protective shield (light grey fields). The protective shield has consisted of air for most simulations to simplify the design.

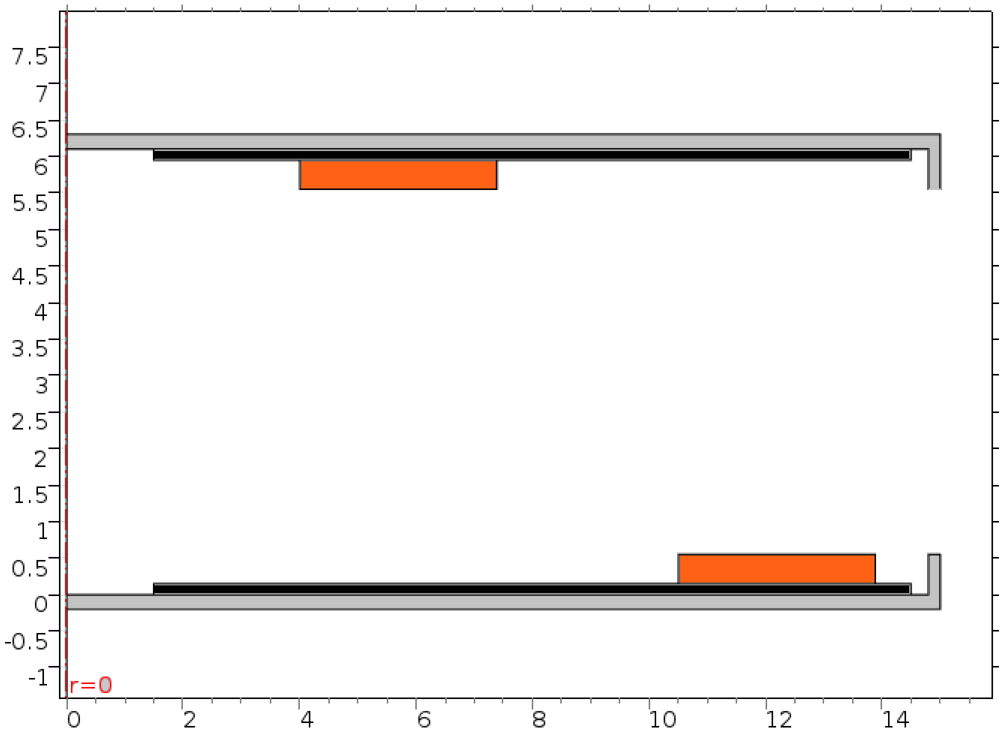

Figure 5.1: The geometry used to simulate the coil design in 2D. The inner orange fields are the copper coils, the black fields in the middle are the ferrite layer and the light grey fields are the shielding. X and Y axes are in centimeters.

The copper wire used for the coils have the dimensions 2.6x4 *mm* and have been placed with its longer side along the y-axis. The primary coil consists of 13 turns, it has a inner radius of 105 *mm* and an outer radius of 139 *mm*. The secondary coil also consist of 13 turns but has a smaller inner radius of 40 *mm* and an outer radius of 74 *mm*.

5.1.2 Analysis of coils in COMSOL

To analyse the power pads in COMSOL the physics module Magnetic Fields was chosen since this includes solutions to all magnetic and electric fields as well as induced voltages and currents. The physics module Electrical Circuit was also added to be able to simulate the electrical circuit which will be connected to the coils. Magnetic fields define Ampère's law for the materials in the model of the coils. The materials used are copper, air and ferrite. The magnetic field in copper and air have a linear relation with a constant relative permeability where the permeability of ferrite has a dependency of the field. In Electrical circuit the circuit components are defined in same way as they would in a circuit analysis software. The currents and voltages in the components can thus be evaluated and analysed in COMSOL as well.

5.1.3 Calculation of inductance in COMSOL

To model the coils of the transformer in a circuit analysis software the inductance of the coils is needed. To calculate the self inductance of a coil in a medium the analytical expression

$$L_{coil} \approx N^2 R \mu_0 \mu_r \left[ln(\frac{8R}{a}) - 2 \right] \tag{5.1}$$

is used where N is the number of turns, R the inner radius, μ_0 the permeability, μ_r the relative permeability and a the radius of the conductor [12]. The calculation of the mutual inductance M is very complicated to do analytically and will only be performed through COMSOL.

As the design of the transfer pads involve a ferromagnetic material the effective inductance of the coils will be affected as well as the mutual inductance. To calculate the inductance for more accurately for the design the FEM software COMSOL Multiphysics is used. To calculate the self inductance in COMSOL the coil is defined and excited by a current and then the magnetic energy can be calculated by

$$W_m = \frac{1}{2} I^2 L \tag{5.2}$$

where W_m is the magnetic energy, I the excitation current and L the self inductance of the excited coil. The mutual inductance M can be calculated by exciting one coil and measure the open circuit voltage in the second coil. The expression for M is

$$M = \frac{V_{oc}}{j\omega I} \tag{5.3}$$

where V_{oc} is the open circuit voltage in the second coil, ω the angular frequency and I is the excitation current.

5.1.4 Verification of analytical and simulated inductance values

To be more confident about the calculated and simulated values a comparison between the analytically calculated values and simulated values from COMSOL Multiphysics and ANSYS Maxwell was performed. The same geometry was created in COMSOL and in Maxwell to compare the accuracy and the same geometry was analytically evaluated. The geometry used in this comparison is not the geometry chosen for the prototype design but is an earlier test design only. In Table 5.1 the values obtained from the three instances is presented.

From Table 5.1 it can be seen that the difference in inductance values between the FEM software is very small, also the analytical values correspond very well with

Table 5.1: Analytically calculated and simulated values of the coil inductance. The geometry used is an early test design not equal to the chosen protoype design.

Without ferrite	Analytical	Maxwell	COMSOL
L1 [μH]	3.7367	3.6376	3.6360
L2 [μH]	1.4560	1.5639	1.5643
M [μH]	-	0.2632	0.2628
With ferrite			
L1 [μH]	-	7.1755	7.1755
L2 [μH]	-	2.9459	2.9631
M [μH]	-	0.9078	0.9097

the simulated ones. The difference between COMSOL and Maxwell is not significant which means that any software will give the results wanted.

5.1.5 Calculated inductance values

With the chosen design of the coils inductance values was calculated in COMSOL to be used for circuit simulations. The values can be found in Table 5.2 and are calculated for the geometry shown in Figure 5.1.

Table 5.2: Calculated inductance values from COMSOL in 2D simulation.

Without ferrite	Inductance
L1 [μH]	71.3
L2 [μH]	24.3
M [μH]	7.0
With ferrite	
L1 [μH]	125.3
L2 [μH]	48.7
M [μH]	19.4

5.2 Coil resistance dependency on frequency

In high frequency systems the resistance of conductors change since the current concentrate at the surface. This is called skin effect and will cause the effective resistance of conductors to increase with the frequency of the current flowing through it. The skin effect is determined by the distance δ which is called skin depth, this depth is defined as the depth below the conductor surface where the current density has decreased by a factor of $e^{-1} = 0.368$ of the surface current density [6]. The skin depth δ can be calculated by

$$\delta = \frac{1}{\sqrt{\pi f \mu \sigma}} \tag{5.4}$$

where f is the frequency of the current, μ is the permeability and σ the conductivity of the material in the conductor [6].

Resistance of a conductor is defined as

$$R = \frac{l}{\sigma A} \tag{5.5}$$

where l is the length of the conductor, σ the conductivity and A the cross-section of the conductor. A is defined as $A = \pi r^2$ for a circular conductor but when the frequency is high and the skin effect affects the surface in which the current flows A can be written as $A \approx \pi(2r - \delta)\delta$ which means the resistance when skin effect is taken into account can be described by

$$R_{ac} \approx \frac{l}{\pi(2r - \delta)\delta} \tag{5.6}$$

where the assumption $2r \gg \delta$ has been made, r is the radius of the conductor and δ is the skin depth. The resistance will thus increase with the frequency as the skin depth decreases, this is true for a solid conductor but might not be valid for our wires.

Litz wire is a bundle of several conductors with a small diameter twisted together which has a total cross-section distributed among them. This results in more uniform distributed current across the wires cross-section. The litz wire is twisted in a way that admits each strand to occupy all positions of the cross-section of the whole wire. This reduces the skin effect as well as the proximity effect which is the effect of nearby windings causing inhomogeneous current distribution over the wire cross-section. By reducing these effects the resulting AC resistance of the wire is lower than in the case of a solid wire [13].

5.2.1 Analytical resistance of the coils

The wire used for winding the coils is Litz wire with 180 strands with 0.2 mm diameter per strand which gives an effective conductive area of 5.655 mm^2. By calculating the length of wire in the coils and then deriving the DC resistance for them by using (5.5) the values 9.965m, 0.0296 Ω, 4.656 m and 0.0138 Ω was calculated for the primary and secondary coil respectively. It should be noted that the length and resistance values have been calculated purely analytically by approximating the size of the coil. The approximate skin depth was also calculated by (5.4) for copper and 100 kHz to be 0.2063 mm which is around two times larger than the radius of each conductor. This means that the effect of skin depth is not applicable according to (5.6) since $2r \approx \delta$ and thus the validity of the equation fails.

5.3 Field shaping and shielding

Magnetic fields can be shaped in different ways by using materials with different properties. Shaping the field is necessary in magnetic circuits and important in IPT applications since stray magnetic fields can induce currents in nearby materials which means that losses will occur, but they can also affect the health of humans.

The parameter that is important in this context is the Relative Permeability (μ_r) which defines materials ability to conduct magnetic fields. The relative permeability in vacuum is 1 and in iron 4000.

If the magnetic field encounters a material with high permeability which is non-conductive the field will be guided inside the material. The field strength and flux will increase inside the material if it is aligned with the field.

Iron which has a high permeability will conduct the field better but since it is conductive eddy currents will be induced also. Repulsion will exist in this case but since the permeability is high enough the repulsion will be overcome by it. The eddy currents will instead contribute to losses and the material will heat up. To minimize these effects in transformers the iron is insulated and thin sheets are pressed together to form a core.

Materials with a low permeability such as aluminium or copper will not conduct the magnetic field well but since the material is conductive eddy currents will be induced. The eddy currents will create a magnetic field in opposite direction of the applied field which causes the external field to be repelled. This means that materials with high conductivity and low permeability work well as shielding since the magnetic field is repelled. The eddy currents induced will give losses but since the material is highly conductive these will be lower than in e.g. iron.

5.4 Layout of the ferrite bars

Ferrite bars is added in the design to control the field and to achieve a good coupling between the coils. The layout of these bars can be optimized and several studies has been done in this area [14]. The design idea of the ferrite layout is a star layout where the ferrite should cover as large area as possible over the coil. The most effective way would be to have a flat round ferrite plate that covers the coil completely but this would be expensive and add alot of weight. The chosen design was derived by placing ferrites in an arrangement that allows as much ferrite as possible to cover the area of the coil. For the primary side which has a larger radius the ferrites was in a star shape with bars originating in the center of the coil and stretch outwards. On the secondary coil the design idea was similar but since the radius of that coil is smaller there is less space in the center. The layout of the ferrite for the secondary pad is very similar but less wide ferrite bars has been used also to be able to use the space more effectively.

6

Resonance circuit simulation

This chapter contains the simulations made in LTSpice with series-series compensation together with a discussion of parallel-parallel compensation which was the first intended topology. The values of the inductances L_1, L_2 and M that are calculated in COMSOL are divided in to leakage inductances $L_{\sigma 1}$, $L_{\sigma 2}$ and magnetizing inductance L_M which are then recalculated to its equivalent values on the primary side using the theory shown in Section 3.3. The winding resistances are calculated using information from COMSOL and by applying the theory from Section 5.2. The compensation capacitors are calculated using the theory from Section 3.5. The load is is modeled as a DC voltage source and is placed behind a rectifier bridge consisting of four diodes. The load is also placed in parallel with a large capacitor to smooth out the load current and voltage. The DC voltage source is simulated with a voltage ranging from 50 V up to 58 V which simulates the internal voltage of the battery which increases as the battery gets charged. The input voltage is supplied by an inverter model which delivers a square wave voltage with adjustable duty cycle.

6.1 Parallel-parallel compensation

When designing the transformer with parallel-parallel compensation, the design was based on the idea of controlling the input current and output current by controlling the frequency. The magnitude of the input current and output current can be found by analysing the circuit in Figure 6.1 which shows the layout of a parallel-parallel compensated circuit. A decrease in frequency from the primary resonance frequency will decrease the reactance of the inductor and increase the current that flows through the primary leakage inductance and the mutual inductance, giving less contribution to the output current. Similarly, an increase in frequency from the primary resonance frequency will increase the current that flows through the primary compensation capacitor since its reactance will decrease with increased frequency. Both cases will lead to a decrease in the output current and an increase in the input current, which will put stress on the power electronics. The coil inductance and the compensating capacitors must be chosen so that a large decrease in output current results in a not so high increase in the input current. However, a decision was made to use series-series compensation due to the complexity in finding the right parameters and because of the high harmonic content present in the input current likely caused by the square wave input voltage.

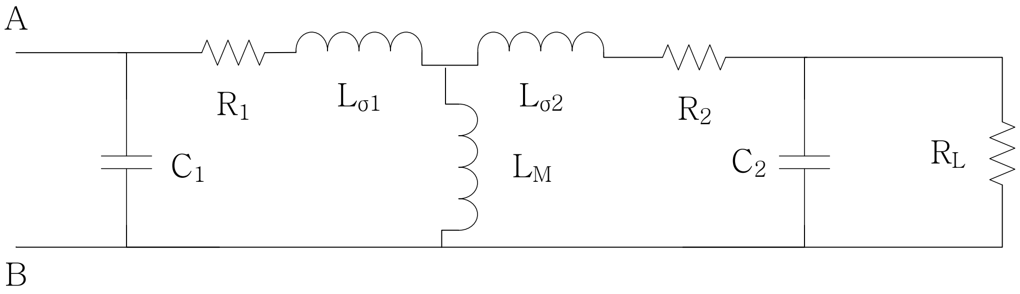

Figure 6.1: The transformer circuit together with parallel-parallel compensation capacitors.

6.1.1 Circuit simulations based on COMSOL for parallel compensation

The simulations for parallel compensation was simulated in Pspice. The main focus in the simulations was centered around the input and output currents and how they changed when the frequency was changed. Figure 6.2 shows a frequency sweep over the RMS value of the input and output currents. The idea is to have normal operation at the resonance frequency of the primary side, which is 68 kHz. This will give an input current of 7 A and an output current of 17 A. When entering constant voltage charging, the output current should be decreased. This is done by increase the frequency, which will increase the input current and decrease the the output current as can be seen in Figure 6.2. The output current will go to zero at about 78 kHz, and at this point the input current will be 15 A which can easily

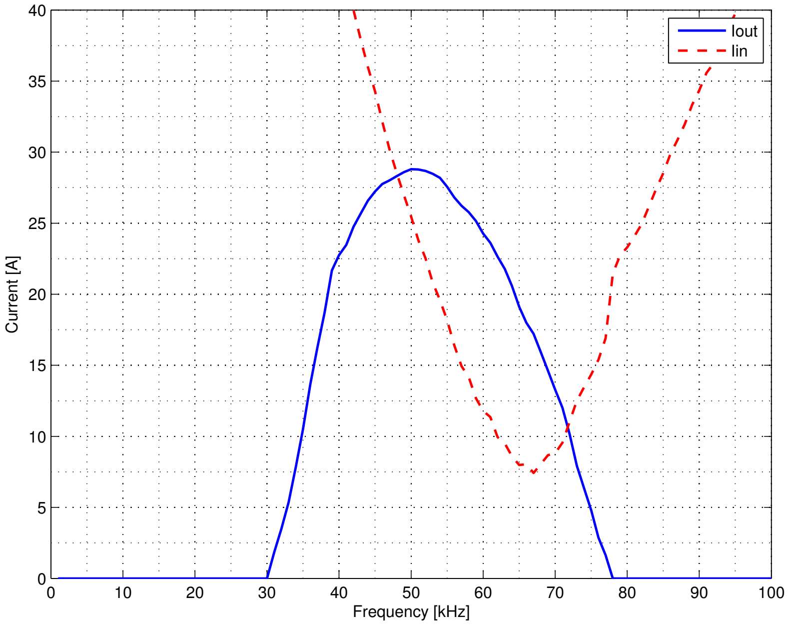

Figure 6.2: The figure shows a frequency sweep when having parallel-parallel compensation

be handled by the power electronics. This shows that it is possible to regulate the output current by changing the frequency. It is however hard to motivate the large input current and the poor power factor that will be present at low output currents. This control method was thereby rejected, and focus was instead put on series-series compensation with duty cycle control.

6.2 Series-series compensation

This section presents the simulations for the series-series compensated charger. The charger is simulated with parameters based on calculations made in COMSOL. The simulations shows that it is possible to transfer 925 W at a DC input voltage of 280 V with a frequency of 100 kHz. The output current is changed by changing the duty cycle. The results motivates that a transformer prototype should be constructed based on the simulations in COMSOL.

6.2.1 Circuit simulations based on COMSOL for series compensation

Figure 6.3 shows the circuit which was used in LTSpice to simulate the final design of the two coils with a 50 V DC source as an equivalent battery load. The input voltage is a 100 kHz, 280 V square wave with a duty cycle of 0.9 which is supplied by the inverter model.

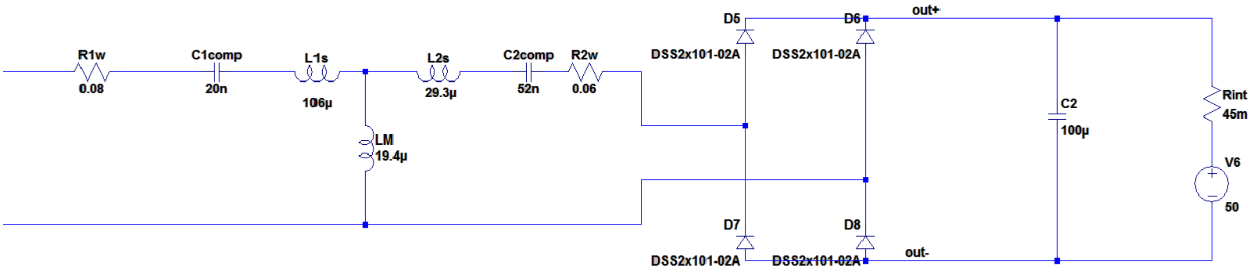

Figure 6.3: The circuit in LTSpice which simulates the two coils with a square wave voltage from the inverter as input and a DC voltage source as load

A sample of the load current is shown in Figure 6.4. The RMS value of the load current is 18.5 A, and by multiplying the load voltage with the load current an output power of 925 W is obtained. The ripple in the load current can be further decreased by having a larger filter capacitor.

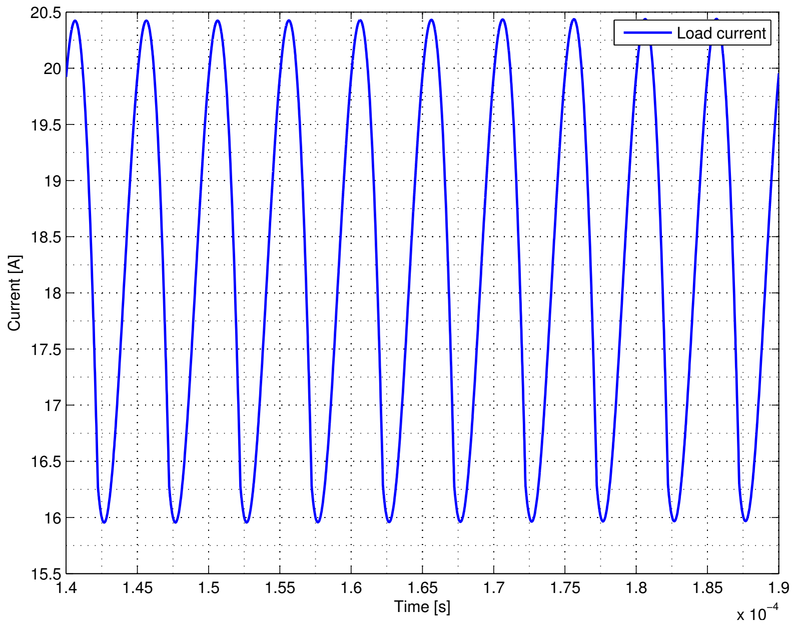

Figure 6.4: The load current when simulating the final design of the coils.

Figure 6.5 shows the input current and the input voltage. It is clear that there is good resonance in the transformer circuit since the current and the voltage are very close in phase. The RMS value of the input current is about 4 A which causes no problems for the power electronics.

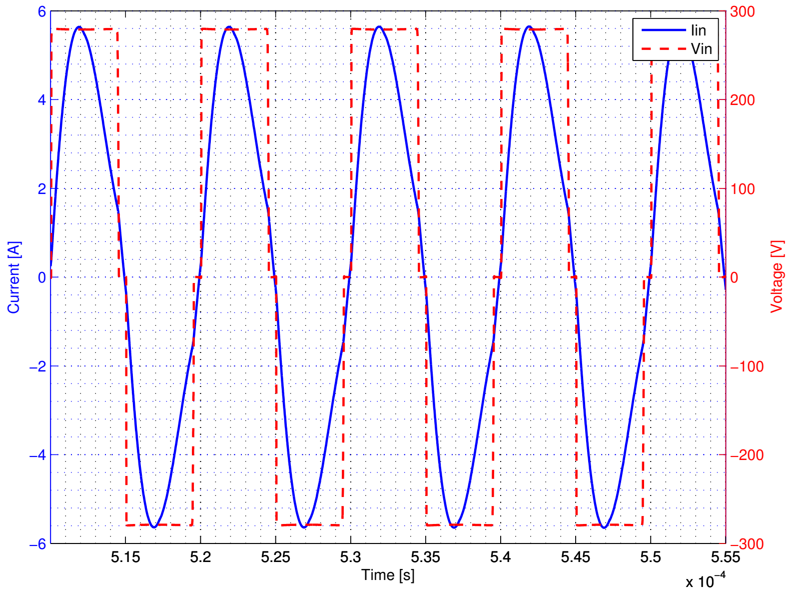

Figure 6.5: The input current and input voltage when simulating the final transformer design.

It is also interesting to look at the input and output current at a range of frequencies. Figure 6.6 shows the RMS value of the input and output current with respect to frequency. It is possible to see that there is three different resonant frequencies between the capacitors and the inductance in the transformer. The local minimum in Figure 6.6 at around 100 kHz corresponds to resonance between the capacitors and the leakage- and mutual inductance which is the point with best efficiency, the two hills corresponds to resonance between the capacitors and other combinations of inductance. It should be noted that the frequency sweep simulation was performed with an ideal sinus voltage source as input voltage and not the model of the inverter.

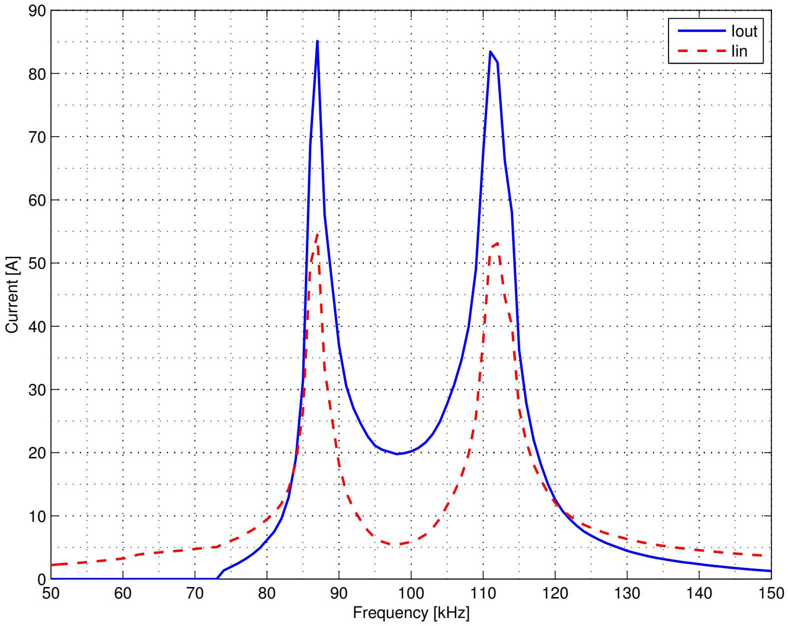

Figure 6.6: A frequency sweep made in Pspice. The resonant circuit has three resonant frequencies which corresponds to the two local maximum and the local minmum in the figure. The transformer is designed to operate at around 100 kHz

7

Construction of prototype

This chapter describes the construction of the two coils of the transformer and how they are fixed to achieve a constant air gap between them as well as how ferrite was added to the coils. The construction of the capacitor banks for the primary and secondary compensation is described and motivated. A description of the system setup is also presented to give an overview of the connections and layout.

7.1 Coils

The coils are designed with only one layer but with several turns. The wire is wound around a center plate with a radius of 40 mm and 105 mm respectively for the secondary and primary coil. The center plate is made of press board and a top and bottom plate is added around it in a sandwich construction. This construction makes the winding of the coil possible while the wire stays in place. Both the primary and secondary coil are made in this sandwich construction with the same outer physical size to achieve alignment between them easily. Both coils consist of 13 turns but with different inner radius to achieve the simulated inductance.

Ferrite was added to the coil pads in a star shape, as can be seen in Figures 7.1a and 7.1b, to maximize the covered area and achieve a good flux path.

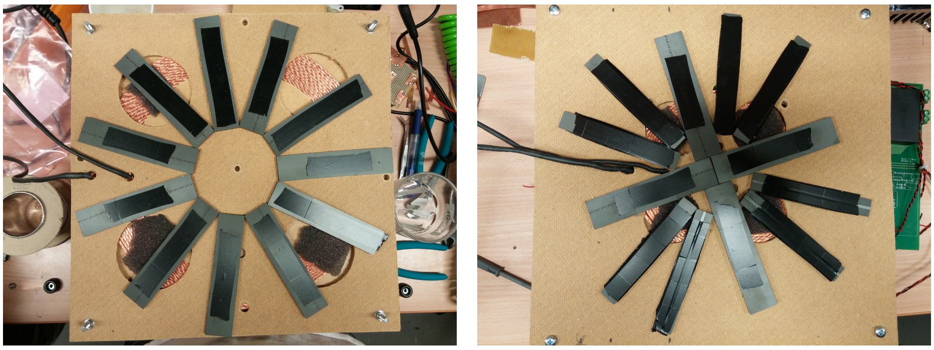

(a) Ferrite layout of the primary coil. Only the larger ferrite plate was used on the primary side since there was enough room in the center of the coil to position them well.

(b) Ferrite layout of the secondary coil. The difference compared with the primary coil is the use of smaller ferrites in some places to achieve better filling of the coil area.

Figure 7.1: Ferrite layout on the two coil pads. Both have a star shape as base but since the secondary has a smaller radius less wide ferrites hase been used to fill the area more effectively.

Two sizes of ferrite plates was used for the coils, the larger one 38x25x3.8 *mm* and the smaller one 22x16x2.5 *mm*. Both ferrite plates was made by Ferroxcube and the same material called 3F3 which has suitable properties for this project. The use of the different sizes can be seen in Figures 7.1a and 7.1b and has been optimized by trial and error. The ferrites is held in place by adding another press board that press the ferrites down onto the coil pad.

To achieve a constant air gap between the coils a kind of cradle has been built by fixing threaded rods in each corner of the coil pads where they are fixed by nuts. This gives a quite accurate way to adjust the gap size between the plates and also results in a good alignment of the two coils through their center. This construction can be seen in Figure 7.2 when both coils are attached with a air gap of 50 *mm* in between and ferrite is added on both coils. The primary coil is on the bottom and the secondary coil is fixed on the rods above the primary.

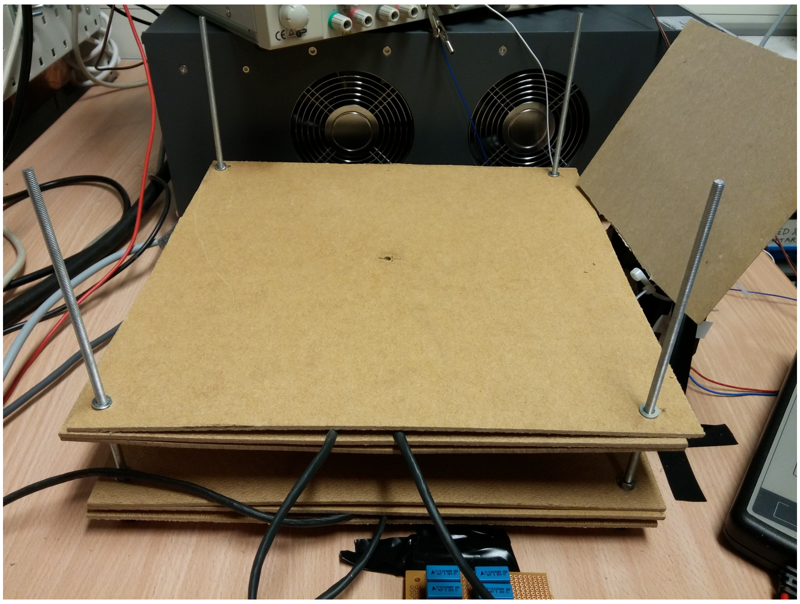

Figure 7.2: Overview of the transformer construction. The two coils are fixed to four threaded rods with the ability to change the distance between them easily. The primary coil is placed on the bottom and the secondary above this with a 50 *mm* air gap. Both coils have ferrite added to them in this figure.

7.2 Capacitor bank

The capacitors are mounted on a strip board and connected together with copper plates. High voltage and high temperature are the two main limitations for capacitors, but these limitations can be dealt with. Figure 7.3 shows the schematics of the primary and secondary capacitor banks.

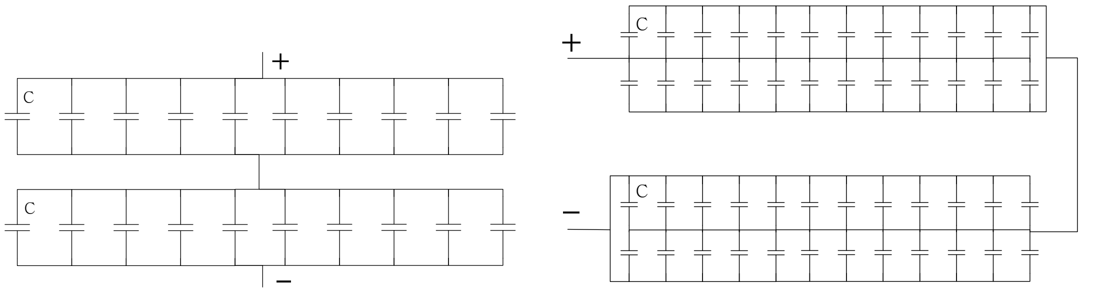

(a) Diagram of the primary side capacitor bank. 10 capacitors parallel connected in series with 10 additional parallel connected. In total 20 capacitors are used.

(b) Diagram of the secondary side capacitor bank. 24 capacitors parallel connected in series with 24 additional parallel connected. In total 48 capacitors are used.

Figure 7.3: Circuit diagrams of the primary and secondary capacitor banks. Each capacitor used has a capacitance of 4.7 nF.

By placing several smaller capacitors in parallel, each capacitor will experience a lower temperature due to the split current. By placing capacitors in series, the voltage will be split and the capacitor bank will be able to handle a higher voltages. The capacitors of the primary and secondary capacitor banks are placed in both parallel and in series to lower the stress. This is also necessary to achieve the calculated capacitance needed for resonance in the circuit. The capacitors used in the system is polypropylene film capacitors with a capacitance of 4.7 nF and a voltage rating of 2000 V DC and 700 V AC. These ratings are valid up to around 100 kHz where the voltage rating starts to decrease rapidly.

7.3 System setup

Figure 7.4 shows the total system of the inductive charger. The inverter is fed directly from a DC power supply, where the input active power is measured. The micro controller is connected to the inverter and a computer. This makes it possible to change the duty cycle of the inverter during charging. The computer is also needed to program the micro controller when for example changes are made to the switching frequency. The output of the inverter is connected to the primary capacitor bank, which is connected in series with the end of the windings of the primary coil. The other end of the primary coil is connected to the second leg of the

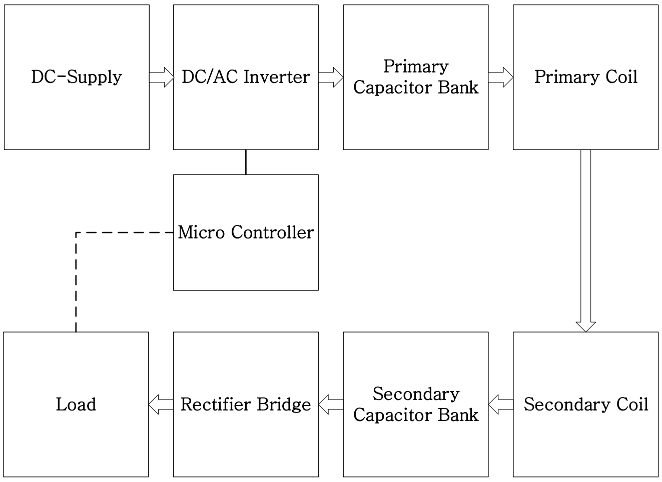

Figure 7.4: The total charger system with each component visible.

inverter. The air gap between the primary and secondary coil is set to 50 mm. The secondary capacitor bank is connected in series with the secondary coil and then the rectifier bridge. The load is connected after the rectifier. A large output capacitor is connected in parallel with the load and an inductor in series with the load to create an output filter to decrease the voltage and current ripple. In Figure 7.5 a picture of the system setup can be seen with each component marked with text. Some fans are also visible in the figure which is used for cooling the system during heavy load.

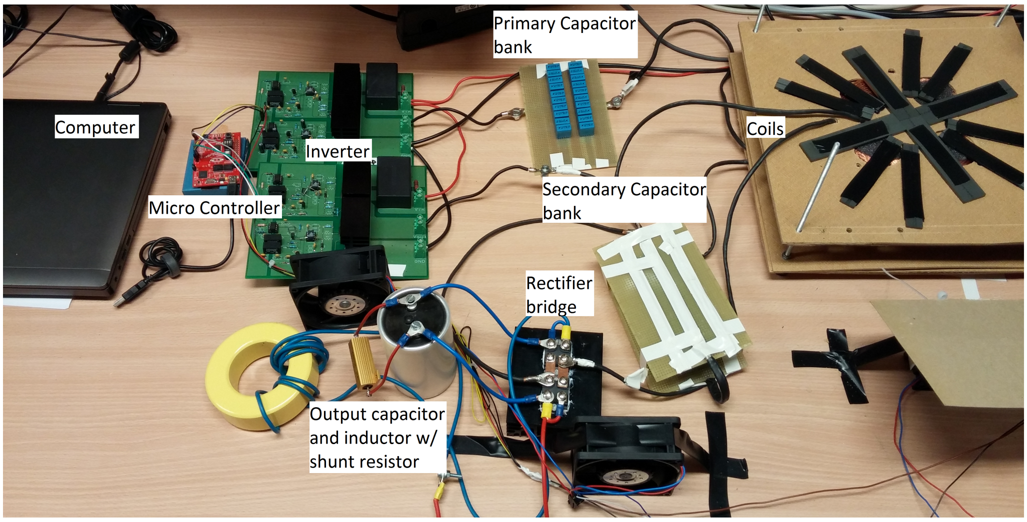

Figure 7.5: An overview of the system setup with each component marked.

8

Measurements and results

The measurement and results chapter is divided into two main sections: measurements on the prototype without ferrite and measurements on the prototype with ferrite. The measurements when no ferrite was added was performed to evaluate how well the simulations corresponded to the assembled charger and to see how much the ferrite affected the power transfer.

8.1 Prototype without added ferrite

This section describes inductance measurements of the coils and load testing off the charger before any ferrite was added. The measurements was performed with an air gap of 50 mm with the two coils perfectly aligned to each other. A load test was performed were 480 W was transferred. A test with higher power was not possible since the capacitors that was available in the lab had a too low voltage rating to be able to handle a full load test.

8.1.1 Inductance measurement

The self inductance of the two coils is measured with a LCR40 passive component analyser. The inductance of the primary coil, L_1, was measured to 75.5 μH and the self inductance of the secondary coil, L_2, was measured to 28.5 μH. The leakage and mutual inductance was determined by a tuning approach instead of direct measurements of the parameters. The primary coil was fed with a 50 V square wave and the secondary coil was held open circuit. The open circuit voltage and the current in the primary coil was then measured. The transformer was then simulated in LTSpice, and the leakage inductance and mutual inductance was changed until the primary current and open circuit voltage was equal to the measured ones. The relation (3.14), which states that the self inductance is the sum of the leakage inductance and mutual inductance, is held constant through out the tuning. The simulation circuit used in LTSpice is shown in Figure 8.1.

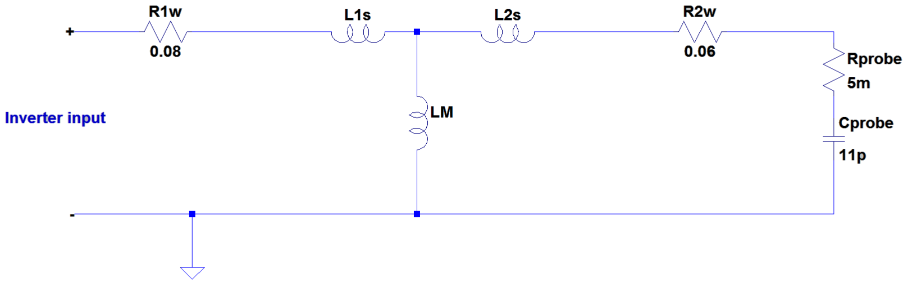

Figure 8.1: The figure shows how the measurements of the open circuit voltage and the primary current was modelled in LTSpice when the mutual and leakage inductance was to be determined.

The voltage probe that measured the open circuit voltage is modelled as a small resistor in series with a capacitor of 11 pF. The real measurements of the primary current and open circuit voltage are shown in Figure 8.2 and Figure 8.3 shows the open circuit voltage and primary current when using the parameters that was acquired by tuning the circuit.

Table 8.1 shows a comparison of the inductance calculated in COMSOL and the inductance that was measured from the real coils. All of the measured inductance was higher than the calculated ones, but the difference was little.

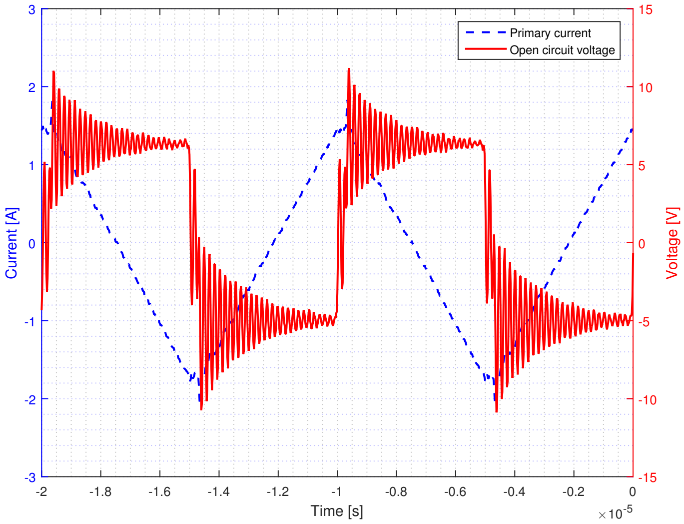

Figure 8.2: The measured values of the open circuit voltage and the current through the primary coil values extracted from the oscilloscope.

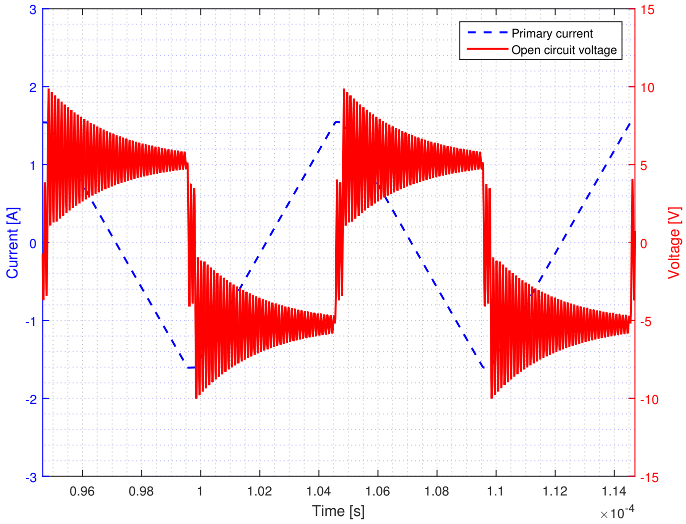

Figure 8.3: The open circuit voltage and primary current from simulations in LTSpice using the values of the leakage inductance and mutual inductance acquired from tuning the circuit.

Table 8.1: Comparison of calculated and measured inductance when no ferrite was added to the coils

Parameter	COMSOL	Measured
$L_{\sigma1}$ $[\mu H]$	64.3	67.5
$L_{\sigma2}$ $[\mu H]$	17.4	20.5
L_M $[\mu H]$	7	8

8.1.2 Load test

The electric circuit of the transformer when testing the power transfer capability of the two coils is shown in Figure 8.4. The test was performed with a 2.66 Ω resistor as load. The primary coil was fed with a 80 V square wave with a 0.95 duty cycle at a frequency of 96 kHz. The injected power was measured to 607 W and the output power was measured to 483 W which gives an efficiency of 80 %.

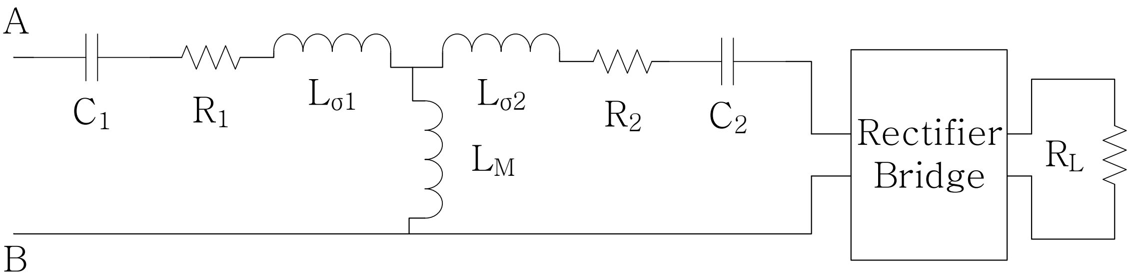

Figure 8.4: The transformer circuit when doing load test of the system without ferrite. The load is in this case a resistance.

The input voltage and input current are shown in Figure 8.5. It can be seen in Figure 8.5 that the input current leads the input voltage and thus, are capacitive.

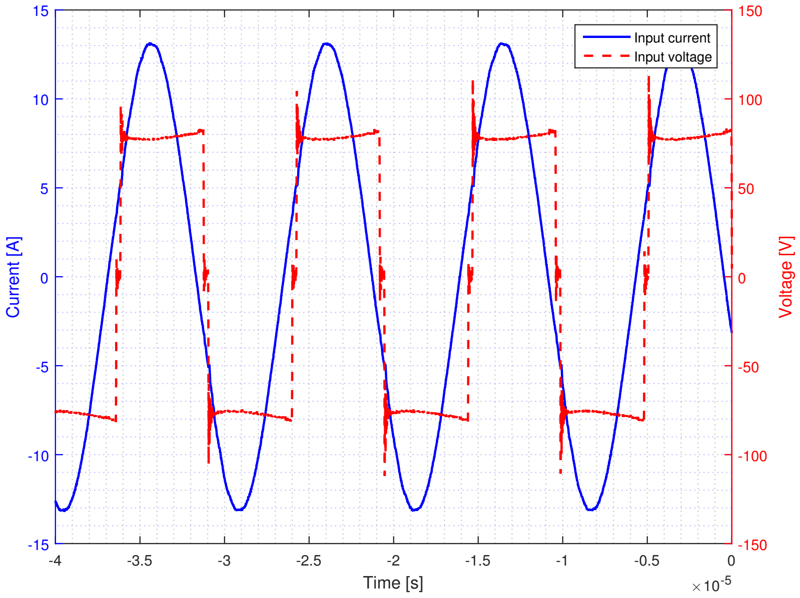

Figure 8.5: The input current and input voltage. It can be seen that the current is capacitive since it is leading the voltage.

This have led to unnecessary switching losses in the inverter since the current must be inductive to achieve ZVS. The load current and load voltage are shown in Figure 8.6.

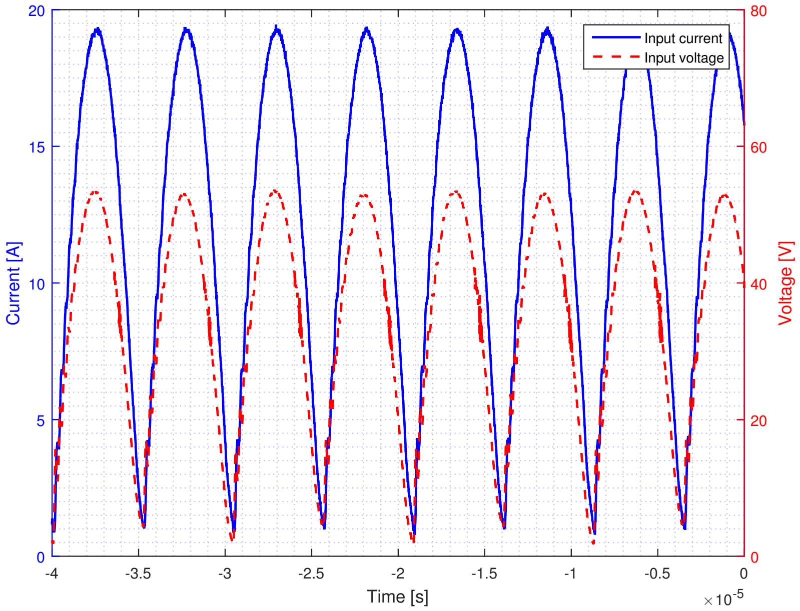

Figure 8.6: The load current and load voltage when transferring 483 W. The load is a 2.66 Ω resistor.

The load current goes down to zero every half period since the test is performed without an output capacitor. The results from the test indicates that the coil design is good and works well with the power electronics. This motivates that further tests should be performed on this design with ferrite added to increase the power transfer capability. All of the load test measurements are specified in Table 8.2.

Table 8.2: Load test measured quantities with values.

Parameter	RMS value
f [kHz]	96
V_{in} [V]	76
I_{in} [A]	9.25
I_{load} [A]	13.2
V_{load} [V]	36.5
S_{in} [VA]	703
P_{in} [W]	607
P_{out} [W]	483
$Efficiency$ [%]	80

8.2 Measured coil resistance

The DC resistance of the coils was evaluated by measuring it in series with a large known resistance. A voltage was applied over the resistances and the current through them was measured. The total resistance was then calculated by the applied voltage and current. From the total resistance the larger known resistance was subtracted and the remaining resistance corresponds to the resistance of the coil. By doing this measurement the primary coil resistance was calculated to be 0.08 Ω and the resistance of the secondary coil was calculated to be 0.06 Ω. This can be compared to the analytically calculated values in Section 5.2.1 which are lower. In Table 8.3 this test is called Measurement 1.

Table 8.3: DC and AC resistance values from calculations and measurements. Measurement 1 was performed with a known resistance in series with the coils and is described further in 8.2.

DC resistance	Analytical [Ω]	Measurement 1 [Ω]	Bode 100 [Ω]
Primary Coil	0.03	0.08	0.04
Secondary Coil	0.018	0.06	0.02
AC resistance	Thermal test [Ω]	Bode 100 [Ω]	
Primary Coil	0.6	0.4	
Secondary Coil	0.4	0.2	

Resistance measurements of the coils was also performed with a vector network analyzer called *Bode 100* which has a frequency test range of 1 Hz to 40 MHz. Both the DC and AC resistance was evaluated using this tool. The results from measuring the resistance with the *Bode 100* was for the primary coil an DC resistance of 39.118 $m\Omega$ and an AC resistance at 100 kHz of 413.304 $m\Omega$. The DC resistance of the secondary coil was measured to 22.652 $m\Omega$ and the AC resistance to 172.477 $m\Omega$ at 100 kHz.

The AC resistance of the two coils was also calculated by a thermal test. The coil was fed a DC current and the temperature was noted after it had stabilized. The coil was then cooled down to room temperature and then fed with an AC current with frequency of 101 kHz since that frequency was chosen for the nominal operating point. The temperature of the coil was then read regularly until it stabilized at the same temperature as when it was fed with DC current. The value of the AC current at which the coil stabilized was lower than the DC current value. The AC resistance was then calculated by assuming that the power loss in the coil was the same for both cases (all power loss was in the form of heat). The resistance could then be calculated by $R_{AC} = \frac{I_{DC}^2}{I_{AC,RMS}^2} R_{DC}$. The AC resistance of the primary coil was calculated to be 0.48 Ω for the primary coil and 0.13 Ω for the secondary coil when using the DC resistance values measured by the apparatus *Bode 100*.

By analyzing the different ways to measure and calculate the resistance of the coils a assumption of the DC and AC resistance was made. For both coils the DC resistance varies between the analytically calculated values and the measured values. The analytical and the values from the *Bode 100* are very similar which lay as a base for the assumption that the DC resistance of the coils are 0.04 Ω and 0.02 Ω for the primary and secondary respectively. When evaluating the losses an estimation for the losses was made for the coils. These estimations resulted in AC resistance values of 0.4 Ω and 0.1 Ω which is lower than the measured AC resistances. By considering the measured values and the estimation done the AC resistance of the primary coil should be around 0.4 Ω and for the secondary coil, 0.2 Ω, which is around 10 times larger than the DC resistance. In Table 8.3 all calculated and measured resistance values are accumulated to give an complete overview.

8.3 Prototype with ferrite

In this section the same measurements done in Section 8.1 was performed as well as more extensive performance tests to evaluate the design. How misalignment of the coils affect the power transfer, the effect of shielding on the system, controllability and the change in resistance in the coils when an AC current is flowing.

8.3.1 Inductance measurement

Inductance measurements were performed on the coils when ferrite was added in the same way as the case without ferrite. Table 8.4 summarizes the values from measurements and the values obtained from COMSOL.

Table 8.4: Comparison of calculated and measured inductance when ferrite was added to the coils

Parameter	COMSOL	Measured
$L_{\sigma 1}$ $[\mu H]$	106	97.3
$L_{\sigma 2}$ $[\mu H]$	29.3	29.2
L_M $[\mu H]$	19.4	17.4

The self inductance of the primary coil L_1 was measured to 114.7 μH and the self inductance L_2 of the secondary coil was measured to 46.6 μH. The lower obtained inductance on the primary coil can be explained by the use of less ferrite compared to the COMSOL simulations. It was however possible to cover the secondary coil with a satisfying amount of ferrite, thus explaining the similarity with the simulated value. The mutual inductance was measured to 17.3 μH which is a little lower the the simulated value. This can again be explained by the lower amount of ferrite on the primary coil. Using (3.14) gives the leakage inductance $L_{\sigma 1} = 97.3\ \mu H$ and $L_{\sigma 2} = 29.2\ \mu H$.

8.3.2 Nominal operating point

The nominal operating point was chosen with respect to output power, input current and efficiency of the total system. The input current must not be to high since this increases the temperature of the MOSFETs. Measurements also shows that a too high input current may lead to saturation in the ferrite and hence, decrease the transferred power. A DC input voltage of 300 V together with a duty cycle of 0.9 and a frequency of 101 kHz for the inverter was chosen. This frequency will not give perfect resonance and the input current will be slightly inductive as seen in Figure 8.7, however not inductive enough to fully achieve ZVS.

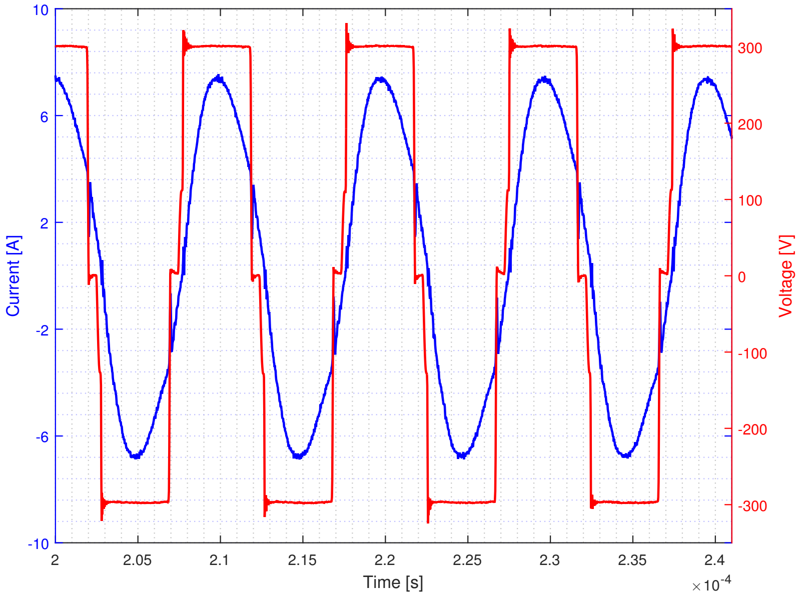

Figure 8.7: The input current and input voltage to the transformer circuit. The current and voltage are out of phase since the nominal frequency of 101 kHz is not the primary resonance frequency.

The efficiency at different frequencies are shown in Figure 8.8. Measurements showed that the input current will increase, and that the efficiency will decrease when going further out of resonance which can be seen in figure 8.8. The efficiency at 101 kHz is 87.3 % and the efficiency at 95 kHz, that corresponds to the poorest operating point in Figure 8.8, is 78.7 %. When operating at the primary resonant frequency which is about 102 kHz, the efficiency was also lower. An explanation to this is that the MOSFETs enters low voltage switching at 101 kHz. The output power at the nominal point is about 1149 W with a battery load voltage of 53.5 V.

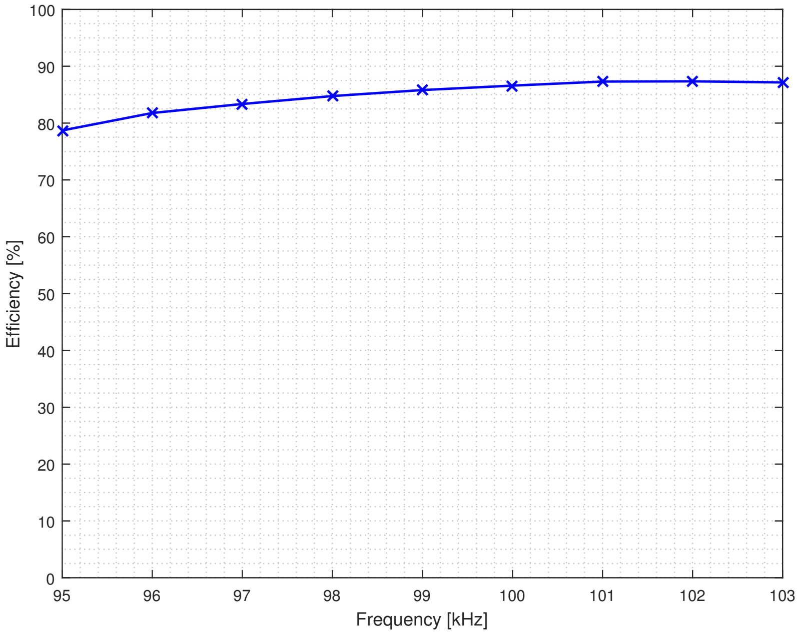

Figure 8.8: The total efficiency with respect to the switching frequency of the inverter. The DC input voltage was 255 V for this test.

The output current and voltage are shown in Figure 8.9.

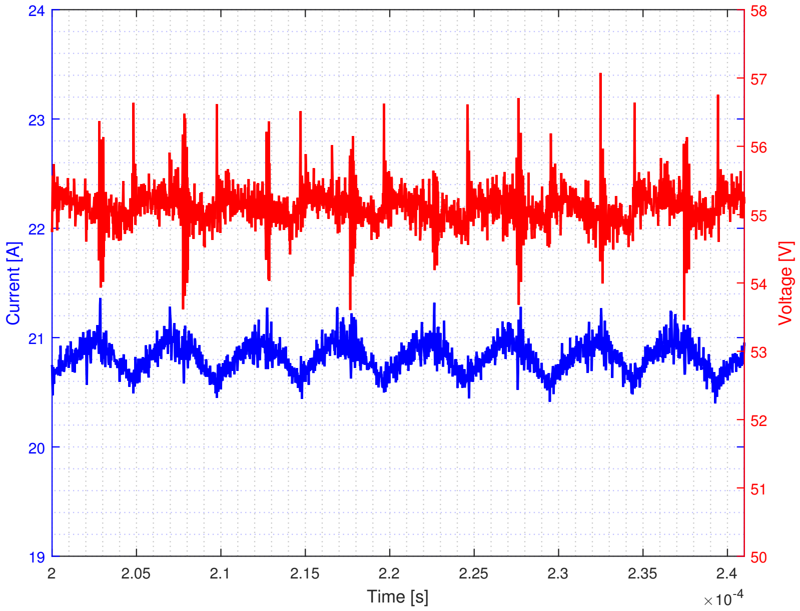

Figure 8.9: A filter that contains a capacitor and an inductor was added after the rectifier, which gives a smoother output current and voltage. The large spikes are noise created by the switching in the inverter.

The battery which was used as a load had a maximum voltage level of 57.6 V, so the ripple in the output voltage must not be to high. To overcome this, a capacitance of 1000 μF and an inductance of 20 μH was added to smooth the output voltage and output current. The curves for the output in Figure 8.9 can be compared with Figure 8.6 which shows the output voltage and current when no output filtering is used. The spikes in Figure 8.9 are switching noise. A summary of the currents, voltages and power at the nominal point is shown in Table 8.5

Table 8.5: Summary of currents, voltages and powers at the nominal operation point

Parameter	Measured
$I_{in,RMS}$ $[A]$	5.1
$V_{in,RMS}$ $[V]$	274
$I_{out,RMS}$ $[A]$	20.8
$V_{out,RMS}$ $[V]$	55.1
P_{in} $[W]$	1356
P_{out} $[W]$	1149
$Efficiency$ [%]	84.7

8.3.3 Losses at nominal operating point

To have a good understanding of the losses in the system each component must be evaluated and its losses calculated. The losses was evaluated when the system was working at the nominal operating point. Calculation of losses can be quite difficult for some parts of the system so an estimation of losses are performed where the calculations are unsure. The first part in the system where losses occur is in the DC/AC inverter. The losses in the inverter consist of conduction losses and switching losses as described in Section 4.1.3 by (4.3) and (4.4). The conduction losses for the inverter was calculated to be 4.21 W when the current $I_{in,RMS} = 5.13\ A$ was measured at the output of the inverter. The parameter $R_{DS,ON} = 0.08\ \Omega$ was found in the data sheet for the switches. By taking the difference between the input power from the DC source and the power at the output of the inverter a power loss of 55 W was calculated. This difference corresponds to the total power loss in the inverter.

Losses in the rectifier bridge was calculated as described in (4.6) to be 33.26 W for the four diodes where $I_{F,AVG} = 20.84\ A$ and $I_{F,RMS} = 20.84\ A$ was measured as the current through the rectifier bridge. If a synchronous rectifier is used instead the losses could probably be lowered a bit in this component although there are other parts that are worse in the system.

The losses in the coils was calculated by using the estimated AC resistance and the RMS current flowing through the coils. The losses was calculated to be 10.5 W in the primary coil and 87 W in the secondary coil. If the losses are summarized a total of 186 W is found. Since the efficiency for the nominal operating point was 84.72 % the total loss should be 207 W which means that 21 W is not accounted for. A part of these losses may have its origin in the ferrite. Other parts of the system where the losses has not been evaluated are the capacitor banks, the DC capacitor with its shunt resistor and the wires connecting the parts. It must be assumed that the remaining losses are spread out between these parts of the system. The distribution of losses are visualized in Figure 8.10 where it quickly becomes clear that the secondary coil is the component in the system with the highest share of the total losses. The losses in the secondary coil contribute with more than 40 %

of the total losses, this can be improved by reducing the AC Resistance. If the litz wire in the secondary coil is changed to one with thinner strands and a larger total conductive area the losses will greatly reduce. The efficiency could probably reach over 90 % in this case.

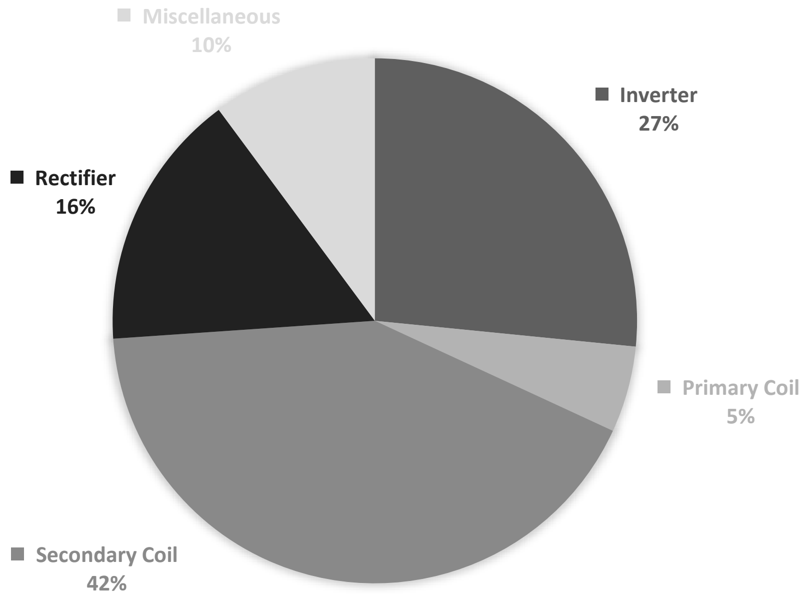

Figure 8.10: The distribution of losses in the system. The miscellaneous part consists of capacitor banks, wires and ferrite saturation.

Figure 8.11 show the operating temperature of the system components during nominal operation. The values are not perfectly accurate since the IR camera assumes the object to be matte with a specific reflectivity. Especially the picture of the coil is inaccurate since the coil wire is quite reflective. It can otherwise be seen that the temperatures of the components are reasonable. The maximum allowed temperature of the rectifier diodes is 150 °C and at this point the temperature is around half. For the MOSFETs the maximum operating temperature is 175 °C which is far above the operating temperature here. The ferrite material that is placed on the coils have a specific power loss minimum at approximately 100 °C where the power loss factor increase at lower or higher temperatures. The temperature of the ferrites was hard to measure but an estimation is around 60 °C at nominal operation.

(a) Heatsink of the MOSFETs.

(b) The casing of one MOSFET.

(c) Temperature of the secondary coil.

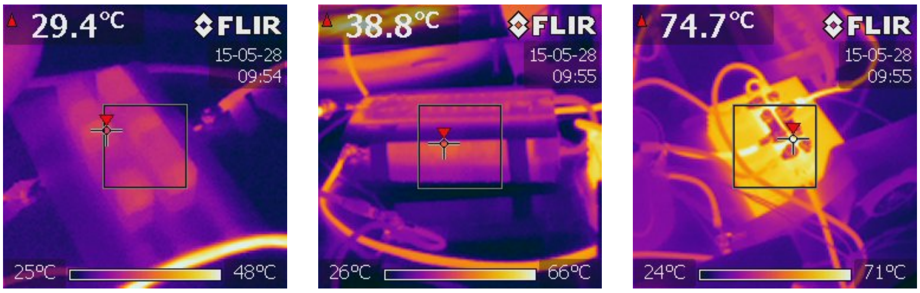

(d) Primary capacitor bank.

(e) Secondary capacitor bank.

(f) Temperature on the rectifier bridge.

Figure 8.11: Temperature measurement of each component at nominal operation. Maximum temperature inside the rectangle is presented in each picture.

8.3.4 Controllability of output power

Since the charger is intended to charge a vehicle battery some sort of control is needed to charge the battery correctly. The most simple way is to change the duty cycle of the voltage which will result in that the RMS of the input voltage will decrease as the duty cycle decrease. As the voltage decrease the current will also decrease and in this way the charging current to the battery can be lowered.

Figure 8.12 show how the input power scale with the duty cycle of the voltage. The test was performed for three voltage levels, 275 V, 300 V and 325 V to see how the input voltage affect the system performance. The duty cycle is varied between 0.1 and 0.95. Figure 8.13 illustrate the output power in respect to the voltage duty cycle. The data is gathered for three voltage levels, 275 V, 300 V and 325 V as in Figure 8.12.

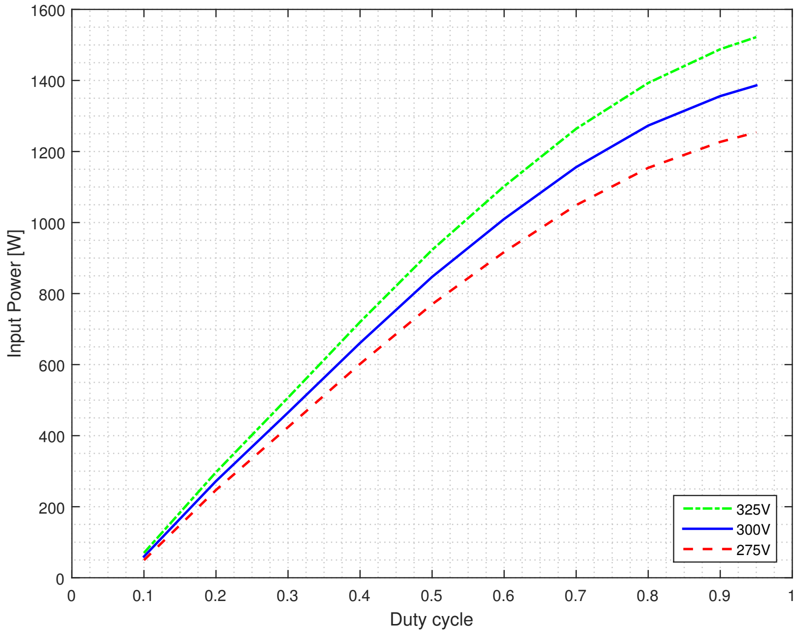

Figure 8.12: The input power to the system as a function of the voltage duty cycle for 275 V, 300 V and 325 V input voltage. The input power increase quite linear but for higher duty cycles a decline can be seen in the curves.

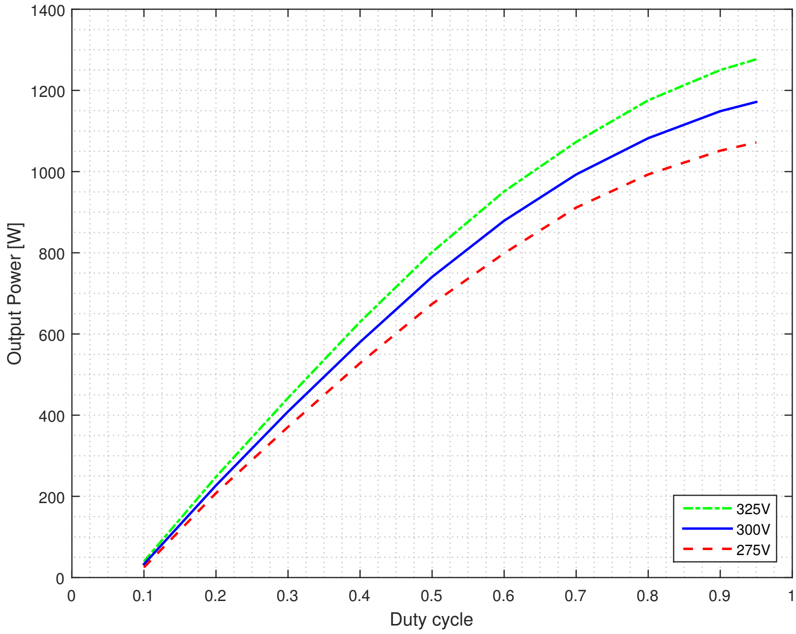

Figure 8.13: The ouput power which is transferred to the battery. The three curves correspond to the three tested voltage levels. The same behaviour as for the input power can be seen here as well.

The behaviour is quite linear but the derivative of the curves is declining as the duty cycle increase. The reason for this might be that for high duty cycles the current will be high and thus the magnetic flux will be high. This may lead to losses inside the ferrite. This problem does not occur when the current/duty cycle is low. The input power and the output power have the same behaviour across the duty cycle range and it can be seen in Figure 8.14 that the efficiency is quite linear from 0.3 duty cycle to 0.95 duty cycle but some decline after 0.7 occur. Figure 8.15 provides a zoom of Figure 8.14 to show the actual efficiency values more clearly.

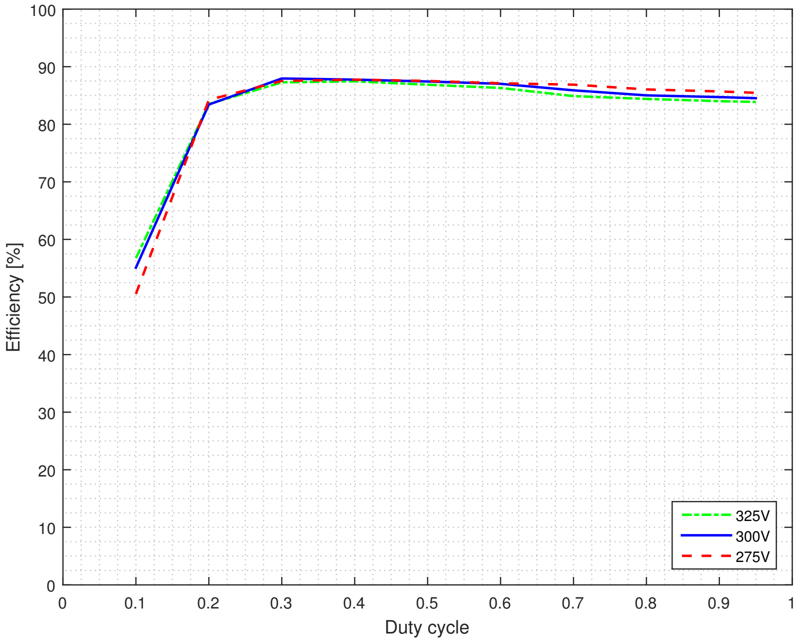

Figure 8.14: The efficiency of the system when a sweep of the voltage duty cycle is performed.

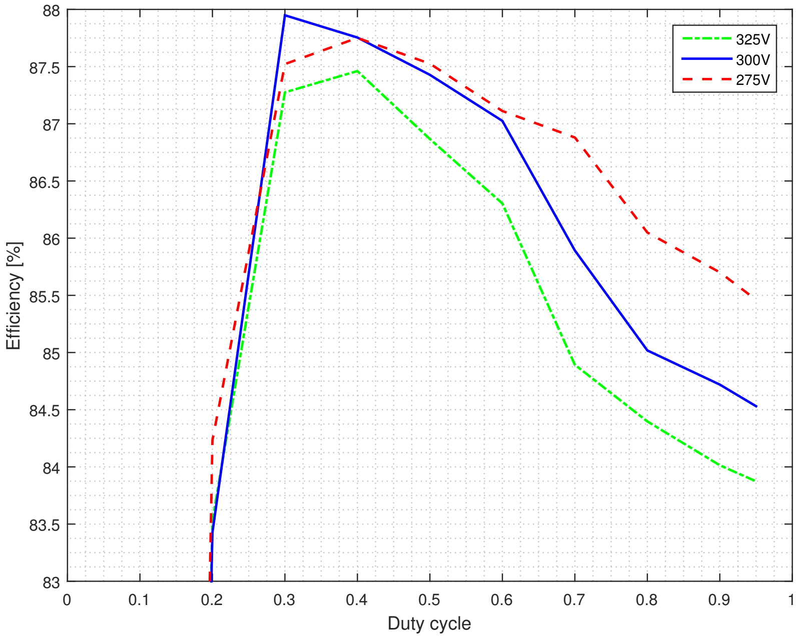

Figure 8.15: A zoom in on the efficiency curves for the three voltage levels (275 V, 300 V, 325 V) tested to visualize the difference in efficiency more clearly.

If a zoom in on the efficiency is done it can be seen that the maximum efficiency of ≈ 88 % is achieved at 0.3 duty cycle and then it is declining over the higher duty cycle range down to $\approx$ 84 % depending on the input voltage. It can also be seen that for a lower input voltage the efficiency is more stable over the range compared to a higher input voltage, this is likely caused by the higher current which introduce higher saturation losses in the ferrite. The chosen nominal point is a duty cycle of 0.9 at an input voltage of 300 V, this curve achieves the highest efficiency of $\approx$ 88 % at 0.3 duty cycle and the lowest efficiency of $\approx$ 84.6 % at 0.95 duty cycle.

8.3.5 Misalignment and changes in gap

Tests was performed on the transformer when the two coils was misaligned to each other and when the gap between the two coils was increased. The two coils are designed to have a gap of 50 mm between them. A misalignment as well as an increased gap distance will lower the mutual inductance and increase the leakage inductance, thus lower the magnetic flux from the primary coil that links with the secondary coil. This will increase the input and output currents which will lead to a larger power transfer, and thereby lower the efficiency of the transformer. Apart from this, the whole self inductance of each coil will change since the coils are coupled and this affects the self inductance of each coil. The self inductance of each coil decrease with about 6 μH when the gap distance is changed from 50 mm to 100 mm. The percentage reduction for the self inductance on the primary coil is 5 % and about 12 % for the secondary coil. This means that resonance on the primary side will be almost unaffected since the percentage reduction of the self inductance of the primary coil is low and that series-series compensation is a linear function of leakage and mutual inductance. Since the self inductance is dependent on the geometry, a different design of the coils would give a different change in self inductance. The input current and input voltage to the transformer circuit for perfectly aligned coils is visible in Figure 8.16. It is possible to see that the power factor is almost one at perfect alignment by visually comparing the input current and voltage.

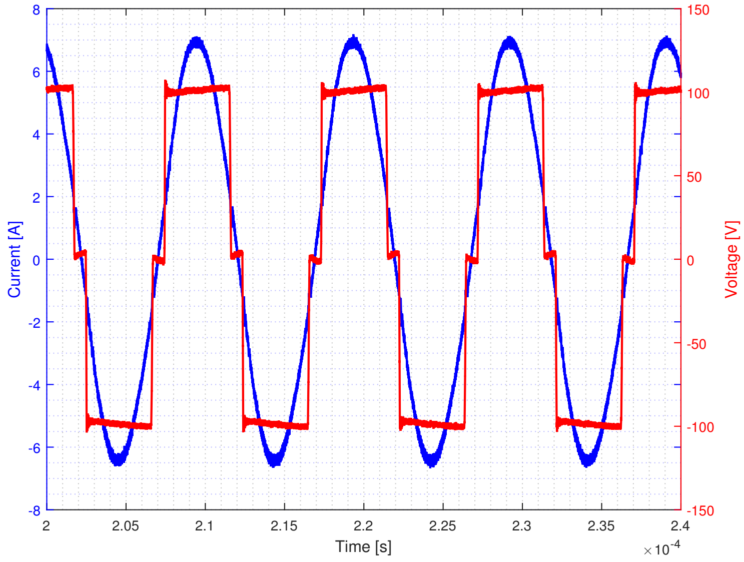

Figure 8.16: The input current and voltage to the transformer circuit at perfect alignment in horizontal direction and a gap of 50 mm.

Figure 8.17 show the input current and voltage when the coils are misaligned 100 mm. The input current increase as the misalignment increase and is here about two times higher than in the perfect case. Figure 8.18 show the input current and voltage when there is a 100 mm gap between the coils. It can be seen that the input current increase and that the phase angle between the current and voltage change. It should be noted that the change in self inductance is negligible for gap distances larger than 100 mm.

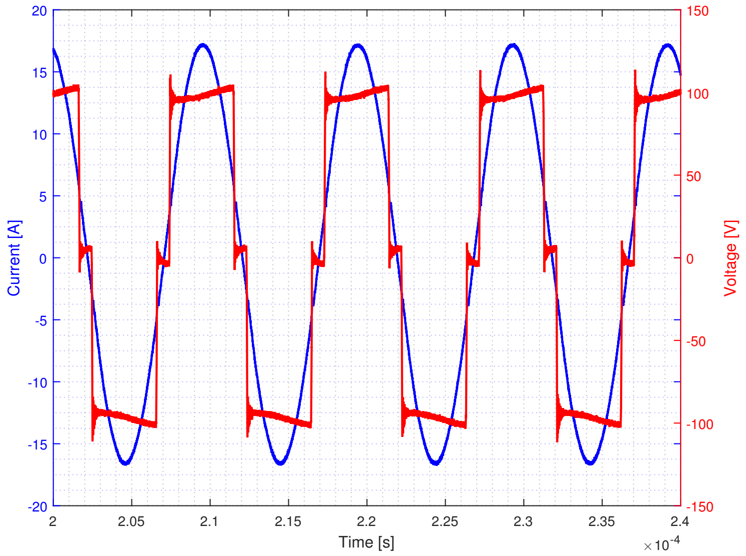

Figure 8.17: The input current and voltage to the transformer circuit at 100 mm misalignment.

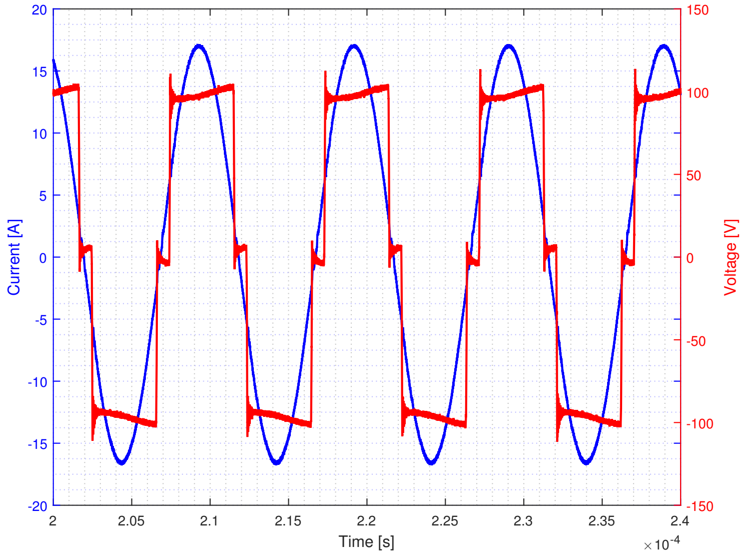

Figure 8.18: The input current and voltage to the transformer circuit at 100 mm gap.

The gap tests was performed by increasing the gap between the coils in steps of 25 mm, and the misalignment tests was performed by displacing the coils in steps of 50 mm. A DC link voltage of 100 V, 0.9 duty cycle, and a frequency of 101 kHz was used in both tests. The low DC-link voltage is motivated by the high currents that is present when the mutual inductance is low. Figure 8.19 shows the efficiency and output power with respect to the gap between the two coils. As seen in the figure, the efficiency decreases from 87.3 % down to 80 % when there is a gap distance of 100 mm.

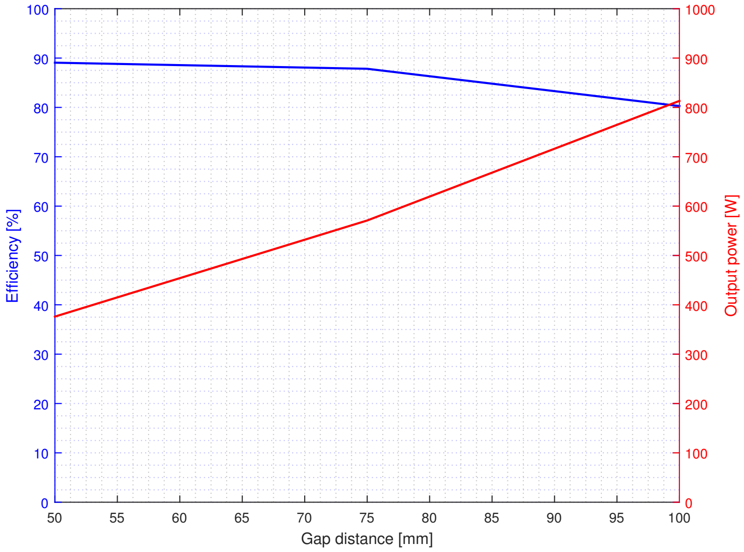

Figure 8.19: The total efficiency with respect to the gap between the two coils. 50 mm is the normal operation point. The output power is also visible in the figure.

Similarly, the efficiency with respect to the amount of misalignment is shown in Figure 8.20. Here, a 100 mm misalignment will cause a drop of 10 % units in efficiency down to 80 %.

The problem with misalignment is the large current that will flow in the primary coil and thereby the power electronics. The end points that was used in these tests are close to the maximum misalignment that are allowed, more misalignment will put to much stress on the power electronics. Since the DC-link voltage of the charger at normal operation is 300 V, the duty cycle of the inverter must be decreased to about 0.3 in order to keep the currents down. By doing this, it is possible to have 80 % at 100 mm misalignment which is good.

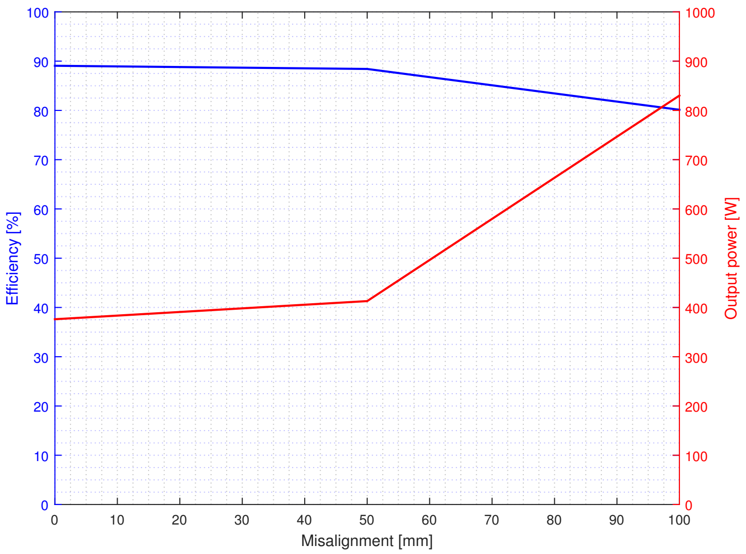

Figure 8.20: The total efficiency with respect to the horizontal misalignment between the two coils. The output power is also visible in the figure.

8.3.6 Effects of shielding

Shielding is needed in high power inductive charging applications to keep the surroundings clear from leakage magnetic fields. The effects of shielding was tested by placing an aluminum plate directly on the receiving pad and 50 mm above the receiving pad when the DC-link voltage was put to 200 V. These measurements was then compared to the case when no shielding was present. Figure 8.21 shows the total efficiency of the charger with respect to the position of the plate. As can be seen, the efficiency will decrease as the plate is placed closer to the pad. As seen in Figure 8.21, the shield is preferably placed some distance above the receiving pad to keep the efficiency high.

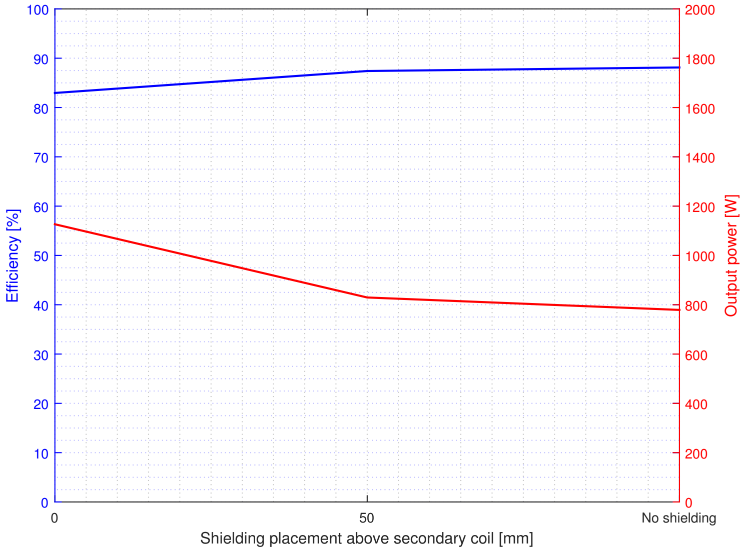

Figure 8.21: The shielding plate was positioned at 0 mm and 50 mm above the secondary coil. This is also compared with no shielding present on the secondary coil.

Figure 8.22 shows the input current and input voltage when the shielding plate is placed just on top of the receiving pad.

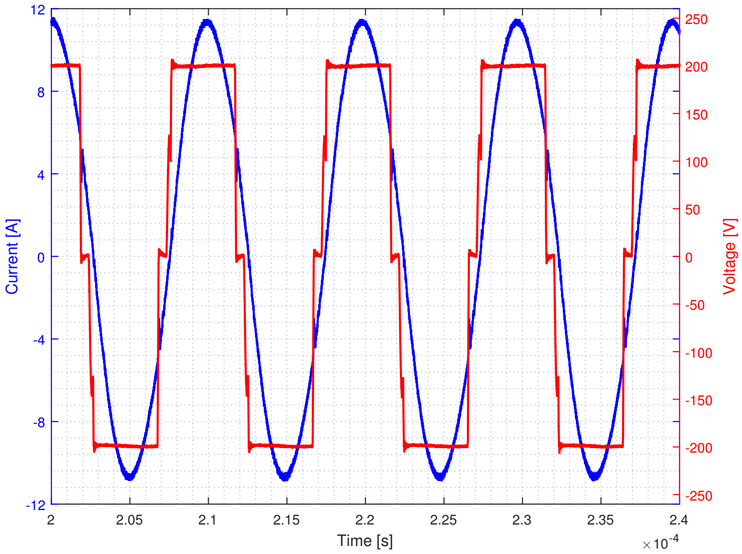

Figure 8.22: The shielding plate is placed just on top of the receiving pad.

Figure 8.23 show the current and voltage when the shielding plate is placed 50 mm above the receiving pad.

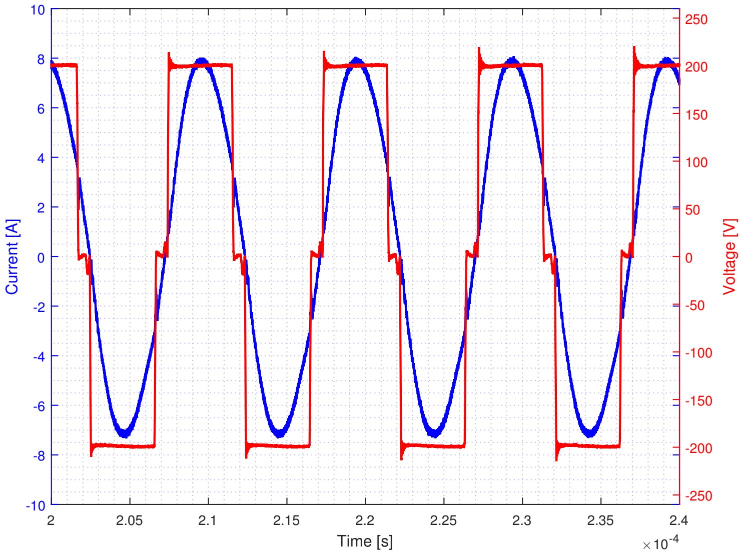

Figure 8.23: The shielding plate is place 50 mm above the receiving pad.

Figure 8.22 and Figure 8.23 can be compared to Figure 8.24 where no shielding is present. By comparing the figures it is clear that the power factor does not change when adding a shield. The mutual inductance will however decrease and this will increase the input current and the overall transferred power for the same DC-link voltage.

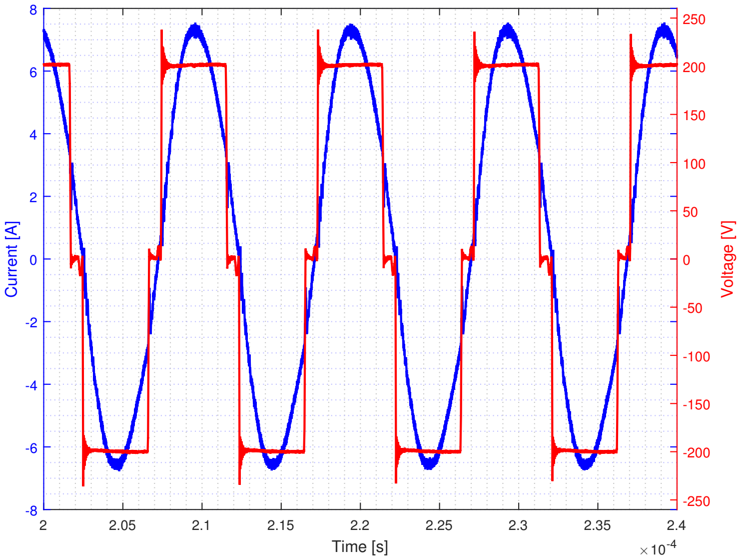

Figure 8.24: No shielding plate is present

8.4 Weight and cost analysis

For the system to be a viable option as a real product both cost and weight are important factors. The weight is especially important for the receiver part since this will add weight to the vehicle. The weight of the coil cradle with ferrite is approximately 3.7 kg but this includes the press board that holds together the structure as well as the threaded rods which the coils are fixed to. The estimated weight of the secondary coil is around 1.5 kg, together with the rectifier bridge and the DC-link filter the total weight on the secondary side should be approximately 2.5 kg. The weight of the vehicle mounted parts are therefore not higher than a traditional conductive charger. Table 8.6 summarizes the cost and weight of the system components. In the table the weights are either measured or estimated from data sheet specifications so the weight will be lower since surrounding structure and similar things are not considered.

Table 8.6: Weight and cost summary. The weights are either measured or estimated from specifications from data sheets.

Component	Cost [SEK]	Weight [kg]
Inverter	2500	0.75
Micro controller	155	-
Capacitor banks	710	0.65
Rectifier bridge	360	0.076 (w/o heatsink)
Coil wire	100	0.76
Ferrite bars	380	0.302
DC-link capacitor and inductor	510	0.6
Total	4815	3.14

The cost is important to consider if the product is to have any prospect to establish on the market. Since the system is a prototype the cost will be relatively high and the estimated cost are calculated at single component level. If the system should reach production the cost for more or less all parts can be reduced since components can be bought in bulk. In Table 8.6 the cost for each part of the system as well as the total cost is presented. The price for components have been taken from several online retailers and are estimations.

9

Conclusion

The aim of this thesis was to show the possibilities of inductive charging for electric vehicles. The project has resulted in a working prototype that can transfer power across an air gap of 50 mm to charge a battery. For the system to charge a Li-ion battery correctly the charging current needs to be controlled. The system can control the charging current by manually changing the duty cycle of the AC voltage that is applied to the circuit. The charger can transfer approximately 700-950 W with an efficiency of more than 87 % which is well above the aim of 800 W with 80 % efficiency. The system also reaches a maximum efficiency of almost 89 % at lower power levels. It can also transfer higher power at lower efficiency, 1200 W at 84 % has been tested. If the losses in the system is minimized the maximum efficiency could reach over 90 %. The size of the onboard receiver was limited to the available space on the vehicle and the resulting size should be within these limits. The system has although not been mounted and tested on the vehicle.

Tests performed shows that the efficiency of the charger will decrease if the coils are misaligned to each other. The large current that are present at misalignment can be lowered by lowering the duty cycle. Some kind of shield against leakage magnetic fields is needed if the charger are to be used on the commercial market. The tests performed with an aluminium shield shows that the efficiency will be 87 % at lower input voltages than nominal if the shield is placed about 50 mm above the receiving pad.

The system is has a total cost of 4815 SEK, but one must consider that it is a prototype and the cost can thus be decreased if the system would be assembled in larger scale. The weight of the transmitter is not that important since it will be a fixed part on the ground. The weight of the receiver however should not be large as unnecessary weight added to a vehicle is unwanted. The estimated weight of the vehicle mounted parts total to 2.5 kg which is not significantly more than an onboard conductive charger. This is a positive aspect since the inductive charger will not add more weight than a conductive charger to the vehicle.

Since the system was able to charge a battery but also transfer power to a resistive load we believe that the technology can be used in a wide variety of applications. Not only charging of electric vehicles but also for hospital equipment or other small to medium power applications.

10

Future work

- For the system to be autonomous a current control should be implemented that receives a feedback signal from the BMS for which current the battery need. This should be implemented by using a PI-controller or similar which control the duty cycle of the voltage which will affect the input and output current to the battery as the BMS decides. The control would need the measured charging current and the reference current from the BMS to function.

- The charging system should be wireless thus communication between the transmitter and receiver is needed. We believe that this could be done by using bluetooth or wifi modules on either side to transfer the signals. A study needs to be performed though to see that the switching frequency does not interfere with the communication so the signal is distorted.

- To increase the efficiency of the system the secondary coil need improvement. This could easily be done by choosing a litz wire with a thinner strands and a larger conductive area which should lower the AC resistance of the coils.

- For the prototype to become a commercial product research into safety standards must be done to create a well packaged product. The size of the inverter can be reduced by using more conductive layers and the capacitor banks can also be reduced in size if a circuit board with an effective layout is printed. The coils can not be reduced in size much but can be packaged better so the thickness will decrease a bit at least. How to effectively incorporate shielding must also be evaluated further.

- To comply with future standards the design could also be remade to transfer higher power, suggestively 3.3 kW. This will probably be the standard for home chargers for electric vehicles and is therefore very interesting to study.

Bibliography

[1] Joseph A. Angelo. *Encyclopedia of Space and Astronomy.* Infobase Publishing.

[2] C.K. Lee, W.X. Zhong, and S.Y.R. Hui. Recent progress in mid-range wireless power transfer. In *Energy Conversion Congress and Exposition (ECCE), 2012 IEEE*, pages 3819–3824, Sept 2012.

[3] International Energy Agency. Key world energy statistics.

[4] David Ferris. How wireless charging will make life simpler (and greener), July 2012.

[5] P. Sathe. Strategic analysis of inductive charging for global electric vehicles (ev) market - executive summary, April 2014.

[6] David.K Cheng. *Field and Wave Electromagnetics.* Addison-Wesley publishing company inc.

[7] S. Chopra and P. Bauer. Analysis and design considerations for a contactless power transfer system. In *Telecommunications Energy Conference (INTELEC), 2011 IEEE 33rd International*, pages 1–6, Oct 2011.

[8] Strålsäkerhetsmyndigheten. Strålsäkerhetsmyndighetens allmänna råd om begränsning av allmänhetens exponering av elektomagnetiska fält (ssmfs 2008:18), 2008.

[9] Undeland T.M Mohan, N and R.P William. *Power electronics.* John Wiley and Sons, INC.

[10] Clemson University Vehicular Electronics Laboratory. Integrated circuit emc.

[11] Steven Keeping. A review of zero-voltage switching and its importance to voltage regulation, 2014.

[12] Frederick.W Grover. *Inductance Calculations.* Dover Publications.

[13] M. Bartoli, N. Noferi, A. Reatti, and M.K. Kazimierczuk. Modeling litz-wire winding losses in high-frequency power inductors. In *Power Electronics Specialists Conference, 1996. PESC '96 Record., 27th Annual IEEE*, volume 2, pages 1690–1696 vol.2, Jun 1996.

[14] M. Budhia, G.A. Covic, and J.T. Boys. Design and optimisation of magnetic structures for lumped inductive power transfer systems. In *Energy Conversion Congress and Exposition, 2009. ECCE 2009. IEEE*, pages 2081–2088, Sept 2009.